Production system to form, cut, and join by using a press machine for continuous carbon fiber-reinforced thermoplastic sheets

Production system to form, cut and join by using a press machine for continuous carbon fiber reinforced thermoplastic sheets

D. Tatsuno[1], T. Yoneyama[1], K. Kawamoto[2], M. Okamoto[2]

[1]Faculty of Mechanical Engineering, Institute of Science and Engineering, Kanazawa University
Kakuma, Kanazawa, Ishikawa, 920-1192, JAPAN
Email:dtatsuno@se.kanazawa-u.ac.jp

[2]Komatsu Industries Corp.
1-1, Shinmachi, Oonomachi, Kanazawa, Ishikawa, 920-0225, JAPAN

Abstract

To build a processing method for textile carbon fiber reinforced thermoplastic (CFRTP) sheets, a production system to form, cut and join the sheets by using a mechanical servo press machine was developed and examined. The system's problems were analyzed and attempts were made to solve them through a series of processes. In press forming, the effects of sheet geometry, fiber orientation, and slide motion on the forming of the variant-cross-sectional-beam, which has a narrow and wide part, were investigated. In addition, the shear-cutting method was chosen trimming the unnecessary region of the variant-cross-sectional-beam. For the joining process, a thermal welding method that uses a heating-plate was chosen. The closed-sectional-beam was fabricated by thermally welding a pair of the variant-cross-sectional-beams. Finally, the potential of the production system for textile CFRTP sheets using the mechanical servo press machine was discussed.

Introduction

Carbon fiber-reinforced thermoplastic (CFRTP), which is a thermoplastic resin impregnated with carbon fibers, has several advantages such as high mechanical strength per weight, short processing time because of its property of melting when heated and solidifying when cooled, and ease in joining them. In particular, CFRTP reinforced by continuous fibers has extremely high mechanical strength. In recent years the trend to develop low-energy-consumption vehicles using CFRTP is significant [1]. Therefore, the demand for processing technologies for CFRTP are increasing. To realize the production system for CFRTP, it is essential to build a series of processes including fabrication of the material, forming the material into the desired shape, cutting, and joining.

Several methods for forming CFRTPs have been studied. A commingle method involves placing the fabric made of commingled yarn of carbon and thermoplastic fibers in a mold, heating the mold to melt the thermoplastic, and applying pressure to impregnate the thermoplastic in the carbon fibers [2,3]. Further, a film-stacking method involves placing a carbon fiber fabric and thermoplastic film alternately in between the rubber diaphragms, and applying heat and pressure to impregnate the thermoplastic to the fabric [4]. A reactive processing involves the placement of a carbon fiber fabric without resins into a mold, injecting the monomer into the mold, impregnating the monomer in the fabric, and polymerizing the monomer [5]. All these methods have the advantage of formability because the carbon fiber fabric to be formed is not impregnated with resin. However, the impregnation process requires considerable time because the molten thermoplastic has high viscosity. Stampable sheets, on which the thermoplastic is impregnated in the fabric, are now available in the market. The stamping method involves heating the stampable sheets to melt the thermoplastic, and applying pressure and cooling the stampable sheets using a mold. This method has an advantage: the time in which the material remains in the mold could be significantly shortened, thus resulting in high productivity. Rubber mold or diaphragm are used as a mold to apply pressure to the stampable sheets [6-8]. However, due to the flexibility of the material of these mold, the surface roughness or shape accuracy of the formed product is poor. Using metal matched dies gives good surface quality and good mechanical properties [9-11]. The effects of stamping pressure and die temperature on the mechanical properties of the product are studied [12-14].

Cutting CFRTP is essential process to trim the products after demolding. Abrasive water jet cutting, laser cutting, milling and sawing are studied for cutting thermoset CFRP [15-19]. In contrast, study on the cutting method for thermoplastic composites are limited. Cutting CFRTP using laser is studied [20, 21]. Shear-cutting method, which has been utilized for cutting sheet metal is studied for cutting CFRTP [22, 23]. Shear cutting method has the advantages such as tools are simple, cost is low, cutting time is short and cutting time is independent to the cutting length of the product. Therefore, high productivity is expected.

The joining method of CFRTP is roughly classified as follows: adhesive bonding, welding, and mechanical fastening [24]. In terms of joining, the advantage of CFRTP is that it can be joined by welding with the combination of heat and pressure. To melt the thermoplastic matrix of CFRTP,

ultrasonic method [25-27], infrared method [28], resistant heating of the heating element [29], induction heating [30, 31] are studied. Disadvantage of these methods is that it need special tools to melt the resin.

In this study, a series of processes were developed for forming, cutting and joining CFRTP sheets by using a mechanical servo press machine, as shown in Figure 1.

The press forming method, which involves the heating of a stampable sheet and cooling it under pressure by using a metal matched die and the press machine is considered in this study. The target shape of the press forming machine is a variant cross-sectional-beam with a narrow and wide part. The effect of sheet geometry, fiber orientation, and slide motion on the quality of the press-formed part are investigated. The distinguishing characteristic of our press forming process is that the stacked stampable sheets are consolidated simultaneously with press forming. The consolidation process involves the stacking of stampable sheets of a single layer, heating of the stacked sheets, press forming and consolidating the sheets under the pressure, and cooling them. Consolidated stampable sheets consists of multi layers, which is generally used in stamping process, de-consolidates when they are heated before the forming. They need to be re-consolidated when they are formed with the pressure [32]. Therefore it is same as to use non-consolidated stampable sheets. The advantage of using non-consolidated stampable sheets is that the consolidation process to prepare consolidated stampable sheets can be eliminated.

The shear-cutting method, which is widely used in sheet metal cutting, was chosen for cutting CFRTP in this study. The press-formed variant-cross-sectional-beam is trimmed through shear-cutting by using the shear-cutting die and press machine. The mechanism of shear-cutting the CFRTP sheet is estimated using the cutting load curve and shape of CFRTP's cut edge.

Heating-plate welding, which melts the thermoplastic and cools it under pressure using heating-plate, is also considered in this study. The flange part of the trimmed variant-cross-sectional-beam is welded to another beam by using the press machine and a closed-sectional-beam is fabricated.

This study demonstrates that the mechanical servo press machine have reasonable potential for forming, cutting and joining CFRTP. Generally, hydraulic press machines are used for forming of CFRTP because the hydraulic press machines can maintain constant pressure during forming. Mechanical servo press machines are widely used for sheet metal forming, fine blanking and forging in automotive industries, owing to its high-speed slide motion, precise slide motion control. Exploring CFRTP processing technologies by using a mechanical servo press machine is significant for expanding the use of CFRTP.

Figure 1. Production system using press machine

1. Material and press machine

1. 1 Stampable sheet

The stampable sheet (made by Ichimura Sangyo CO., LTD.) consists of 3k carbon fiber plain woven fabric impregnated with PA6. Figure 2 shows the inner structure and surface of the stampable sheet. PA6 fulfills the fiber bundles as shown in Figure 2(a). Its thickness is 0.2 mm. Figure 2(b) shows sheet surface morphology.

Figure 2. Stampable sheet

1. 2 Press machine

A mechanical servo press (Komatsu Industries' H1F45) was used as the press machine. Figure 3 shows the schematic of the press machine. The slide stroke is 100 mm and maximum press load is 450 kN. The slide moves by the servo motor and the linkage. Its position (the height from the top of the bolster to the bottom of the slide measured by the displacement gauge) is the target value for controlling the slide position. In this study, this slide motion is called position control. The slide position and the press load were recorded in the data collection system of the press machine. Further, the air die cushion is installed under the bolster and generates up to 35 kN load in the upward direction.

Figure 3. Schematic of the press machine structure

1. 3 Press forming die

A near-infrared heater was used for heating the stampable sheet before press forming.

Figure 4 shows the schematic of the press-forming die. The sheet holder is used to prevent cooling of the hot stampable sheet when it is placed onto the die, and to prevent wrinkling during the forming. The sheet holder is lifted by the die cushion load generated by the air pressure of the die cushion. When the slide descends, the stampable sheet is formed while being held by the upper die and sheet holder. The die does not have heaters or cooling channels. Figure 5 shows the schematic geometry of the variant-cross-sectional-beam (referred to as "beam" hereafter), with 32 mm height and 3 mm thickness. The width of the beam varies from 58 to 108 mm at its middle. It is one-third the length of the front-side member, which is the front impact-absorbing component of an automobile.

Figure 4. Schematic of press forming die

Figure 5. Geometry of the variant-cross-sectional-beam

1. 4 Press forming condition

Fifteen 0.2 mm thick stampable sheets were stacked and heated up to 280℃. The number of

sheets were determined to match thickness to 3 mm which is the thickness of the beam. Next, the hot sheet was manually transferred to a lower die as quickly as possible and the slide was descended. The slide position is maintained at the bottom dead center for 30 s. The slide speed from the initiation of the sheet deformation to the bottom dead center (30 mm in distance) is 100 mm/s. The die cushion load is 5 kN, and the die is at room temperature. The press pressure (maximum press load divided by the projection area of the lower die 31280 mm^2) is 7 MPa.

Generally, a press load cannot be given as the target value to the mechanical servo press machine. The press load during the press forming is determined by the position of the bottom dead center of the slide. Figure 6 shows the assignment details of the bottom dead center. The position of the bottom dead center, for which the clearance between the upper and lower dies is equal to the thickness of the product to be press formed during a no-load operation, is used as the reference position for defining other positions of the bottom dead center. The distance from the reference to the actual position of the bottom dead center is referred to as the additional stroke. The force used to compress the stampable sheets is not effective when the upper die descends to the reference bottom dead center. If the additional stroke is applied under this condition, the upper die would descend further. The force used to compress the sheets is generated by the application of an additional stroke, with the reaction force pushing the slide upward according to the compliance of the press machine frame. Thus, the sheets are not compressed by the same amount of force as the additional stroke under no-load operation conditions. A larger additional stroke increases the pressure on the sheets. The additional stroke was determined to apply the desired pressure to the sheet during press forming. The additional stroke affects the porosity of the inner structure of the product [33].

Figure 6. Assignment of additional strokes and the actual bottom dead center

2. Press forming

2. 1 Effect of sheet geometry

The formability was evaluated on the three types of sheet geometry shown in Figure 7. Sheet A is tapered from the middle, sheet B is tapered through the sheet, and sheet C has a contour that matches the contour of the die. The fiber direction is parallel to the longitudinal direction of the die.

The widths of the fiber bundles at the side of the beam's neck are stretched or compressed after the press forming of sheet A, as shown in Figure 8(a). Such deformation is small in sheets B and C, as shown in Figures 8(b) and (c), respectively. When the sheet is deformed to the desired shape, the sheet to be deformed to the side of the neck is stretched in the longitudinal direction. The region in which the material remains as the flange part of the neck hinders the stretching. The formability improved by reducing the fibers of this region. Sheet C is the most preferable sheet in terms of formability; however, it is difficult to cut. Therefore, sheet B was used in this study.

Figure 7. Sheet geometry

Figure 8. Difference of fiber deformation owing to sheet geometry

2．2 Fiber deformation

When continuous fibers are deformed into the shape of the beam, the path length of the top fibers and of the fibers coming from the top to the side is different; therefore, the compression of the sheet occurs in the longitudinal direction, as shown in Figure 9 (a).

The fibers at the top of the beam are bended, and compression is observed in the longitudinal direction at the neck part, as shown in Figure 9(b). At the end of the beam, the edges of the 1st and 2nd layers are slipped, indicating that the sheets are drawn into the middle of the beam. The sheet placed at the middle of the sheet holder shifts in the width direction after the forming. In contrast, the fibers touching the lower die are straight. Figure 10 shows the inner structure where the top fibers are compressed; the waviness of the 1st and 2nd layers are increased; however, the remainder of the layers are not deformed in such a manner. The reason for this is still uncertain. One of the possible reasons could be that the fibers that touch the lower die solidify rapidly because of cooling and are not compressed. The microscopic photos of the inner structure in this paper were taken in high resolution using KEYENCE's optical digital microscope VH-5500.

Figure 9. Fiber deformation after press forming

Figure 10. Inner structure (view A). Taken in high resolution using optical microscope

2．3 Effect of holding plate

To prevent the shift of the sheet and the unnecessary deformation of the fibers at the top of the beam during the forming, the holding plate was added in the upper die, as shown in Figure 11. The holding plate suppresses the center of the sheet to the top of the lower die. The maximum pressure of suppression is 0.4 MPa (5 kN where the spring fully compresses divided by the area of the holding plate, i.e., 280 mm × 47 mm).

When the holding plate is used (Figure 12 (a)), the compression of the fibers at the neck cannot be seen. Figure 12 (b) shows the inner structure, in which the deformation shown in Figure 10 does not occur. By using a holding plate, the compression of the fibers is prevented. However, the shift of the sheet still remains. To prevent the sheet from shifting during the forming, a mechanism is needed to generate sufficient force to suppress the sheet from the beginning of its forming.

Figure 11. Mechanism of holding the sheet during press forming

Figure 12. Result of press forming using the die with holding plate

2．4 Effect of fiber direction

When the beam is formed using continuous fibers (Figure 13 (a)), the fibers at the side of the tapering part diagonally orient against the longitudinal direction of the beam. Sufficient mechanical strength cannot be expected because the fibers are diagonal to the longitudinal direction of the beam.

The (-20/70) sheet (Figure 13 (b)), which the fibers are oriented to be parallel to the longitudinal direction of the beam after being formed, was then deployed. The fiber direction was determined from the development view of the beam. The (-20/70) sheet was deployed at the 1st and 2nd layers and the 14th and 15th layers. From the 3rd to 13th layers, the fibers are parallel to the longitudinal direction of the beam.

２．４．１ Result of forming with (-20/70) sheets

The fibers on the top are bended, while the 1st and 2nd layers are shrunk in the longitudinal direction, as shown in Figure 14. The fibers at the side of the tapering part are almost parallel to the longitudinal direction. Further, the fibers that touch the lower die are straight.

Figure 13. Fiber direction of the sheet considering the deformation caused by press forming

Figure 14. Forming result using (-20/70) sheets

２．４．２ Specimen for bending test

To investigate the relationship between the fiber direction and flexure strength, three specimens from the top and one specimen from the side of the tapering part were cut from the beam. The length and width are 60 and 8 mm, respectively. Figure 15 shows where the upper and lower dies touch the top of specimen B and the side of specimen D.

Figure 15 (a) shows the fibers crossing along the longitudinal direction in specimen B with (0/90) sheets only. Figure 15 (b) shows that the fibers are diagonal in the specimen B that includes (-20/70) sheets. In Figure 15 (c), the fibers are diagonal and do not cross along the longitudinal direction in specimen D with (0/90) sheets only. Figure 15 (d) shows that the fibers touching the upper die cross along the longitudinal direction while being curved in specimen D with (-20/70) sheets. In the same specimen, the fibers touching the lower die are parallel to the longitudinal direction and cross completely along the specimen.

Figure 15. Fiber orientation in the specimens in different fiber direction

２．４．３ Inner structure

The inner structure in which the specimens of the flexure test were cut were observed using a microscope. In specimen B with (0/90) sheets (Figure 16 (a)), every fiber in the longitudinal direction crosses along the specimen. In specimen B with (-20/70) sheets (Figure 16 (b)), the fibers in the longitudinal direction in the 1st and 2nd layers and the 14th and 15th layers terminate in the specimen. In specimen D with (0/90) sheets (Figure 16 (c)), the fibers do not cross along the specimen. In specimen D with (-20/70) sheets (Figure 16 (d)), the fibers in the longitudinal direction in the 1st and 2nd layers and the 14th and 15th layers cross along the specimen. The desired fiber orientation is realized by using the sheet in which the fiber orientation is optimum after the forming.

Figure 16. Difference in the inner structure due to the fiber direction. Taken in high resolution using optical microscope

2．4．4 Flexural strength

The three point flexural test was conducted for the specimens shown in Figure 15. The span length was 40 mm and the testing speed was 0.9mm/min. The testing load was applied from where the upper die touched the specimen. In the specimens with the (0/90) sheet, the rigidity of specimen D at the side of the tapering part is lower than that of specimens A, B, and C, as shown in Figure 17 (a). The average flexural strength of specimens A, B, and C is 490 MPa, whereas that of specimen D is 358 MPa, as shown in Figure 17 (c). Specimen D is weak because the fibers do not cross along the specimen as described in section 2.4.2. In specimen with (-20/70) sheets, the rigidity of specimen D is the same as that of specimens A, B, and C, as shown in Figure 17 (b). In addition, the average flexural strength of specimens A, B, and C is 460 MPa, whereas that of specimen D is 469 MPa. Both rigidity and flexural strength improved by using the sheet with optimized fiber orientation.

Figure 17. Result of flexural test in different fiber direction

2．5 Effect of slide-motion

The mechanical servo press has the bottom dead center because the rotational motion of the servo motor is converted to a reciprocating motion by the linkage, as shown in Figure 18 (a). During position control, when the position of the slide is maintained at the bottom dead center during press forming of the CFRTP sheet, the press load decreases with thermal shrinkage due to the cooling of the sheet, as shown in Figure 19 (a). In case of the hydraulic press, the slide stops when the press load reaches the desired load in the slide stroke. The press maintains the desired load and the slide descends further with the thermal shrinkage of the sheet; thus, the hydraulic press maintains a constant load during press forming. The advantages of the mechanical servo press over the hydraulic press include high-speed slide motion and precise control of the slide position.

The load control program, which maintains the desired press load during sheet forming, was installed into the mechanical servo press machine H1F45 used in this study. Figure 18(b) shows the slide motion during the load control operation. Considering the thermal shrinkage of the sheet, the additional stroke of the slide is assigned a larger value than that in the position control operation. First, the slide descends to the switching-position (1.7 mm above the bottom dead center), where the load control operation starts. Until the slide reaches the switching position, it moves with the position control. As the slide reaches the switching position, the load control operation starts, and the slide moves up or down according to the detected press load to match the desired press load. The slide speed until the switching-position is 100 mm/s; the slide moves slower in the region of the load control. The slide keeps descending when it passes over the switching position.

In the position control operation (Figure 19 (a)), the press load decreases after the maximum

load; the press load decreases to 180 kN (5.7 MPa) when the temperature of the middle of the sheet becomes the melting temperature of the resin (230℃). In the load control operation (Figure 19 (b)), the press load reaches the desired value of 220 kN (7 MPa), and then remains at 220 kN. The temperature of the sheet was measured using the 0.25 diameter sheath thermocouple inserted into the notch at the middle of the 8th sheet layer.

The flexural strength at the top is 520–580 MPa in the position control operation, whereas it is more than 600 MPa in the load control operation, as shown in Figure 20. The flexural strength was improved by applying sufficient pressure to the sheet while the resin is in molten state.

Figure 18. Slide motion in the load control operation

Figure 19. Difference between press-load and temperature curves due to slide motion

Figure 20. Difference between flexural strength due to slide motion

3. Shear cutting

The unnecessary part of the beam's flange was trimmed using the shear-cutting die mounted on the press machine. The shear-cutting process consists of placing the beam onto the lower die, descending the slide, and shear cutting by using upper and lower cutting blades while the holder holds the beam's flange with the rubber spring, as shown in Figure 21 (a). The maximum holding load generated by the rubber spring is 35 kN. Figure 21 (b) shows the shear-cutting die. Figure 22 (a) shows that the upper cutting blade attached to the upper die appears as an inverted V when viewed from the side of the blade. The lower cutting blade is straight. The cutting progresses in both the thickness and longitudinal directions, as shown in figure 22 (b). The angle of the tip of the cutting blades is 90°. The clearance between the upper and lower cutting blades is adjustable. The cutting blades are made of hardened SKD11.

Figure 21. Shear-cutting die

Figure 22. Shape of cutting blades

Figure 23 (a) shows the cutting load curve during shear cutting. The parameters of shear cutting are as follows: the clearance c between the upper and the lower cutting blades was c = 0.1 and 0.3 mm, and the slide speed v = 2 and 26 mm/s. The horizontal axis of the graph shows the slide position (height from the bottom dead center). The starting position of cutting is at 8 mm, and the end of cutting is at 5 mm.

Regardless of the clearance and the slide speed, the trend of the cutting load curve is almost the same. When the slide speed is 26 mm/s, the maximum cutting load is 10 kN smaller than when the slide speed is 2 mm/s. It is assumed that the sheet breaks in a brittle manner and the resistance force of cutting becomes small for the slide speed of 26 mm/s.

The position of the cutting blade while shear cutting was estimated according to the cutting load

curve, as shown in Figure 23 (b). From the tip of the cutting blade contacting the sheet until it reaches the center of the sheet, the cutting load increases (1 and 2 in Figure 23 (a)). Then, the cutting load is constant until the tip of the cutting blade reaches the bottom of the sheet (2 and 3 in Figure 23 (a)). Immediately after the tip of the cutting blade reaches the back of the sheet, the cutting load drops to zero (3 and 4 in Figure 23 (a)). It is assumed that the CFRTP sheet breaks before the cutting blade passes through its thickness.

Figure 23. Relationship between cutting load and position of the cutting blade during shear cutting

Figure 24 (a) demonstrates one of the results of shear cutting. The CFRTP beam was trimmed using the shear-cutting method. Figure 24 (b) shows the shape of the cut edge at the section A. The cut edge has smooth region at the upper and bottom halves, and has shaggy region in the middle. The smooth region is called the “sheared face,” assuming that it was generated by shear cutting. Further, the shaggy region is called the “fractured face,” assuming that it was generated by fracturing the fibers. The shape of the cut edge is almost the same for all the conditions chosen in this study.

The shear-cutting process was estimated according to the cutting load curve and cut-edge shape, as shown in Figure 25. The CFRTP sheet bends at the beginning of the cutting (1 in Figure 25). The sheared face is generated at both the top and bottom while the cutting blade descends further (2 in Figure 25). The fibers at the center of the sheet break because of the tension caused by the progress of the cutting blade (3 in Figure 25). The sheet is broken when the sheared and fractured faces penetrate each other. After the cutting blade is removed, the cut edge elastically recovers; the sheared face becomes diagonal and the fractured face is drawn in the sheet.

Figure 24. Result of shear cutting

Figure 25. Estimation of shear cutting mechanism

4. Joining

A pair of the trimmed beam is joined, and the closed-sectional beam is fabricated using the joining die mounted on the press machine, as shown in Figure 26.

The heating plates, which apply pressure only to the flange part of the beam, include cartridge heaters. These plates are heated up to 290℃ and placed on the pair of beams. Next, the slide is descended to the slide position where 0.1 MPa pressure is applied by the springs to the flange part. After the flange part is melted, air is introduced into the die cushion, which is raised to touch the heating plates. The cartridge heaters are then turned off, and the flange part is cooled using the cooling block while 5 MPa is applied by the die cushion.

Figure 27 (a) shows the closed-sectional-beam. Figure 27 (b) shows the inner structure of the flange part of section A. The flange part, where the heating plates contact (joining region), is joined.

On the left of the joining region, some hollows are observed. In this region (referred to as heat-affected region), the resin melted due to heat conduction from the joining region; the deconsolidation then occurred, and the region cooled without pressure, thus forming the hollows. When the heat is applied locally, it is essential to apply pressure to the heat-affected region while cooling.

Figure 26. Joining die

Figure 27. Result of joining

5. Discussion

5. 1 A series of processes utilizing the press machine

The mechanical servo press machine used in this study has the following advantages: high-speed slide motion and precise control of the slide position to the hydraulic press. The machine is widely used for deep drawing of a sheet metal, fine blanking, and forging. The high-speed slide motion is effective for forming a stampable sheet while it is hot. In general, the mechanical servo press cannot operate in load control; however, the load control operation is possible as demonstrated in this paper. In the shear-cutting process, precise control of the slide-motion could effectively control the shape of the cut edge.

5. 2 Press forming

The press-forming process in this study consolidates single stampable sheets during press forming. This study demonstrated that such a method could produce CFRTP products with sufficient mechanical properties. In addition, this method can eliminate the consolidation process to produce multilayered stampable sheets. When a quasi-isotropic laminate is formed, because each layer is separated, less interaction between the adjacent layers, thus reducing wrinkles.

The effects of sheet geometry, fiber orientation, and slide motion on the quality of the product were investigated. The sheets whose contours match the contours of the die have good formability. The decrease in the mechanical strength due to fiber deformation caused by the desired shape can be compensated by using a sheet with fiber orientation optimized after the forming. The mechanical property of the product increases by the load control operation that compensates the reduction in the press load due to the thermal shrinkage during resin cooling.

5. 3 Shear cutting

The shear-cutting method is effective for the cutting of CFRTP. The advantages of shear cutting are as follows: the tool is simple, processing time is short, and processing time is independent of the length of cutting. However, the cut-edge shape must be improved. The shape of the cutting blade and direction of the cutting must be investigated in future studies.

5. 4 Joining

The welding using the heating plate demonstrated in this study is an effective and a much simpler method than the adhesion and mechanical fastening methods. In this study, the die cushion

of the press machine was used for joining. Although the die cushion is generally used to prevent wrinkles in the forming of sheet metal, it is also effective for joining CFRTP, as demonstrated. In the future, the design of the joining die and pressuring method, which preserve the structure at the heat-affected region, must be considered.

6. Conclusion

This paper demonstrated a series of processes, from forming to the joining of CFRTP sheets by using a mechanical servo press machine. In addition, the potential of this process was demonstrated. The propose method agrees with the requirements for the processing technologies of CFRTP of being suitable for a mass-production system, namely, short processing time and low cost. Moreover, it is likely to be preferred if the existing machines or machines familiar to a manufacturer are useful for processing CFRTP. A mechanical servo press machine is widely used in the field of sheet metal forming. CFRTP is expected to be used in automotive industries. Therefore, developed processing technologies for CFRTP using press machine is significant for the growth of CFRTP usage.

Acknowledgements

This study was supported by A-STEP of the Japan Science and Technology Agency.

The author also gratefully acknowledge the work of Mr. Shiozaki and Mr. Nogata.

References

1. K. Friedrich and A. A. Almajid, *Appl. Compos. Mater.*, **20**, 2 (2013).
2. A. Ramasamy, Y. Wang, and J. Muzzy, *Polym. Compos.*, **17**, 3(1996).
3. A. G. Gibson and J.-A. Månson, *Compos. Manuf.*, **3**, 4 (1992).
4. C. Hopmann, M. Hildebrandt, R. Bouffier, and K. Fischer, "Inline-Impregnation – individualized production of thermoplastic continuous fiber reinforced composite parts," *SAMPE Baltimore 2015*, (2015)
5. K. van Rijswijk and H. E. N. Bersee, *Composites Part A: Applied Science and Manufacturing*, **38**, 3 (2007).
6. V. Antonelli, R. Carbone, S. Lindstedt, and R. Marissen, "Pressure Distribution and Surface Quality During Forming of Thermoplastic Composites With a Collection of Rubber Particles As Mould Half," *17th Int. Conf. Compos. Mater.*, (2009).
7. C. M. O'Bradaigh and P. J. Mallon, *Compos. Sci. Technol.*, **35**, 3 (1989).
8. T. Yoneyama, T. Teraoka, and K. Masuzawa, *J. JSTP* , **53**, 613 (2012).
9. J. Chen, J. A. Sherwood, P. Buso, S. Chow, and D. Lussier, *Polym. Compos.*, **21**, 4 (2000).
10. M. Hou, "Stamp forming of fabric-reinforced thermoplastic composites," Polym. Compos., vol. 17, no. 4, pp. 596–603, Aug. 1996.
11. J. Nowacki and M. Neitzel, *Compos.*, **21**, 4 (2000).
12. M. D. Wakeman, P. Blanchard, and J. A. E. Månson, "Void evolution during stamp-forming of thermoplastic composites," *17th Int. Conf. Compos. Mater.*, (2005).
13. M. Hou, L. Ye, and Y. W. Mai, *J. Mater. Process. Technol.*, **63**, 1 (1997).
14. H. Lessard, G. Lebrun, A. Benkaddour, and X. T. Pham, *Compos. Part A Appl. Sci. Manuf.*, **70**, (2015).
15. A. Alberdi, A. Suárez, T. Artaza, G. A. Escobar-Palafox, and K. Ridgway, *Procedia Eng.*, **63**,(2013).
16. T. M. Yue and K. C. Chan, *Polym. Compos.*, **19**, 1 (1998).
17. D. . Shanmugam, F. . Chen, E. Siores, and M. Brandt, *Compos. Struct.*, **57**, 1 (2002).
18. M. Haddad, R. Zitoune, H. Bougherara, F. Eyma, and B. Castanié, *Compos. Part B Eng.*, **57**, (2014).
19. R. Teti, *CIRP Ann. - Manuf. Technol.*, **51**, 2 (2002).
20. P. Hansen, S. R. Pérez, R. Staehr, and P. Jaeschke, "Quasi-Static and Fatigue Evaluation of Laser Machined Cf-Pps and Cf-Pei Composites," *20th Int. Conf. Compos. Mater.*, (2015).
21. F. Caiazzo, F. Curcio, G. Daurelio, and F. M. C. Minutolo, *J. Mater. Process. Technol.*, **159**, 3 (2005).
22. K. Ogi, and S. Yashiro, "Effect of Temperature and Clearance on Shear Cutting Behaviors in CFRP Laminates," 2003. *20th Int. Conf. Compos. Mater.*, (2015).
23. N. Koga, and S. Huo, *J. JSTP*, **57**, (2016).
24. A. Yousefpour, M. Hojjati, and J.-P. Immarigeon, *J. Thermo Plast. Compos.*, **17**, (2014)
25. S.-J. Liu, I.-T. Chang, and S.-W. Hung, *Polym. Compos.*, **22**, 1 (2001).
26. I. F. Villegas, *Compos. Part A Appl. Sci. Manuf.*, **65**, (2014).
27. G. Palardy, and I. F. Villegas, "*Ultrasonic Welding of Thermoplastic Composites with Flat Energy Directors: Influence of The Thickness of the Energy Director on the Welding Process,*" *20th Int. Conf. Compos. Mater.*,

(2015).

28. I. De Baere, K. Allaer, S. Jacques, W. Van Paepegem, and J. Degrieck, *Polym. Compos.*, **33**, 7 (2012).
29. D. Stavrov and H. E. N. Bersee, *Compos. Part A Appl. Sci. Manuf.*, **36**, 1 (2005).
30. T. J. Ahmed, D. Stavrov, H. E. N. Bersee, and A. Beukers, *Compos. Part A Appl. Sci. Manuf.*, **37**, 10 (2006).
31. S. Pappadà, A. Salomi, J. Montanaro, A. Passaro, A. Caruso, and A. Maffezzoli, *Aerosp. Sci. Technol.*, **43**, (2015).
32. L. Ye, Z. R. Chen, M. Lu, and M. Hou, *Compos. Part A Appl. Sci. Manuf.*, **36**, 7 (2005).
33. T. Yoneyama, D. Tatsuno, K. Kawamoto, and M. Okamoto, *Int. J. Autom. Technol.*, **10**, 3 (2016).

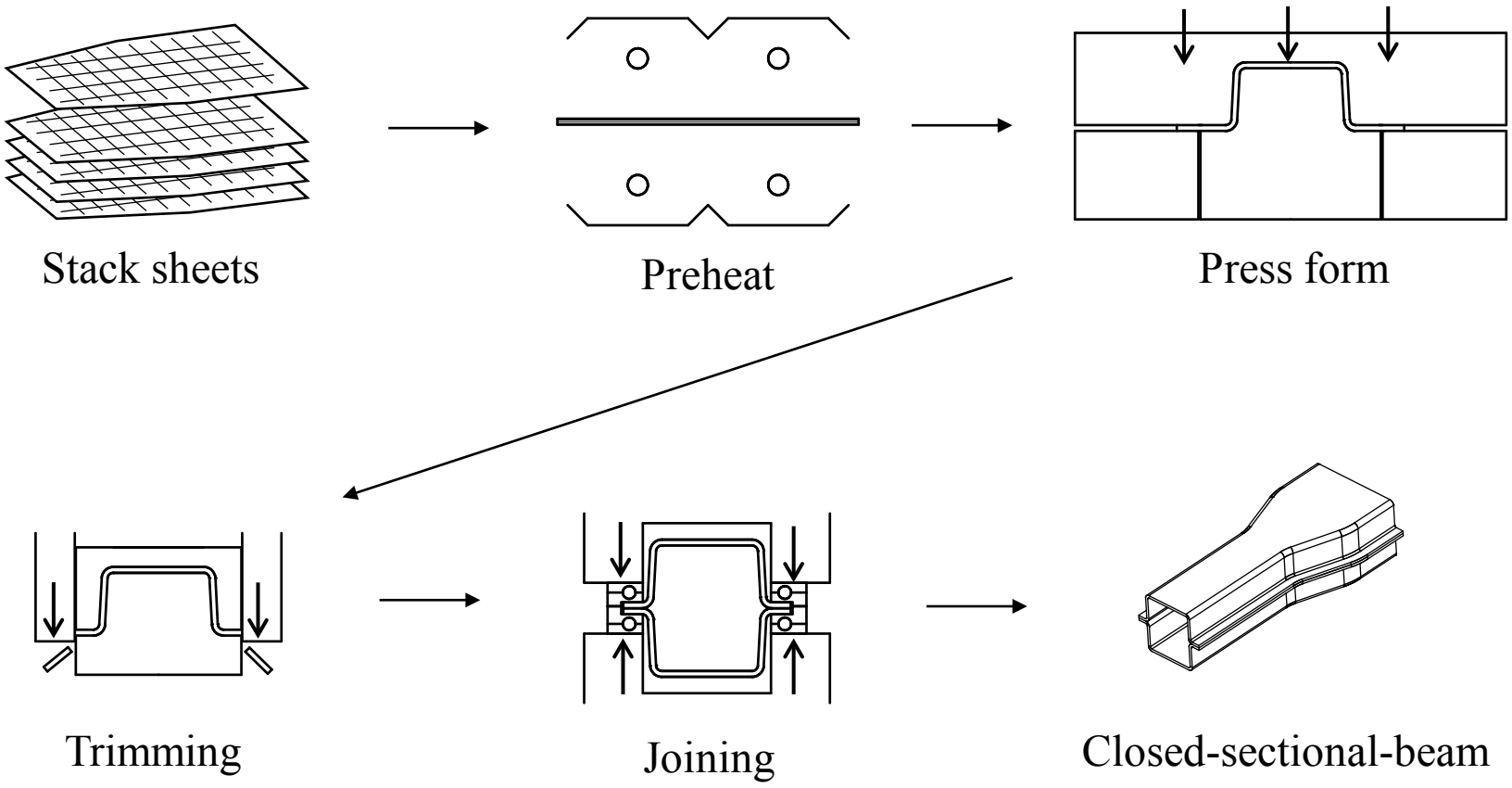

Figure 1. Production system using press machine

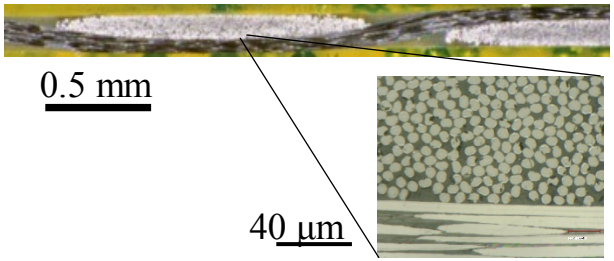

(a) Inner structure of sheet

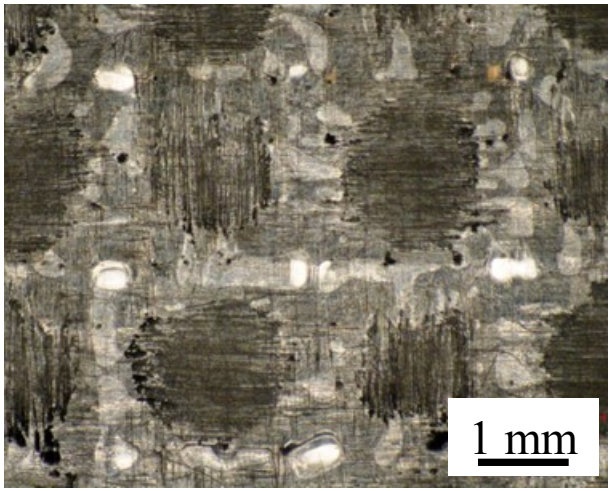

(b) Sheet surface

Figure 2. Stampable sheet

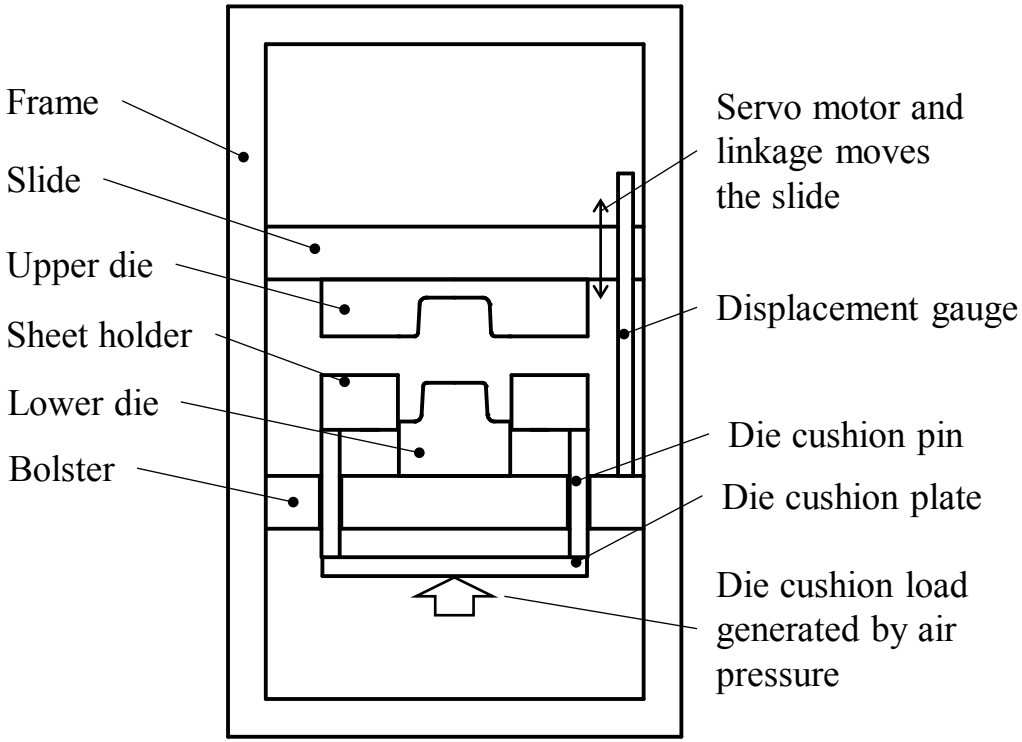

Figure 3. Schematic of the press machine structure

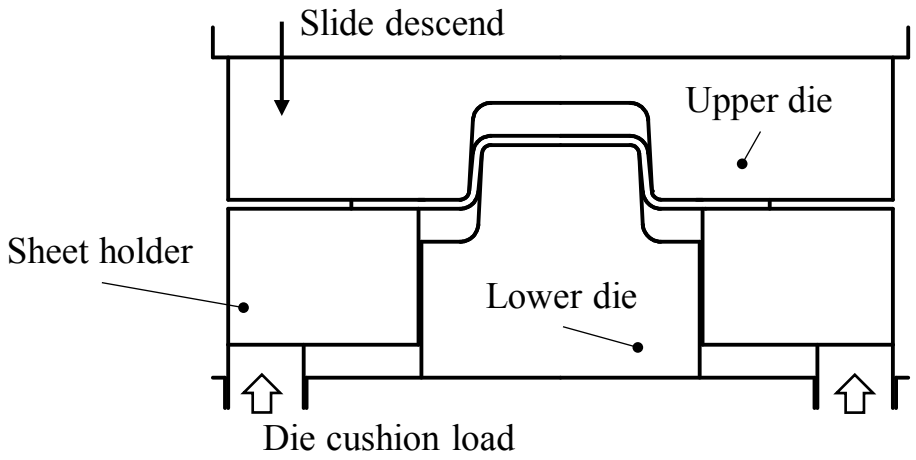

Figure 4. Schematic of press forming die

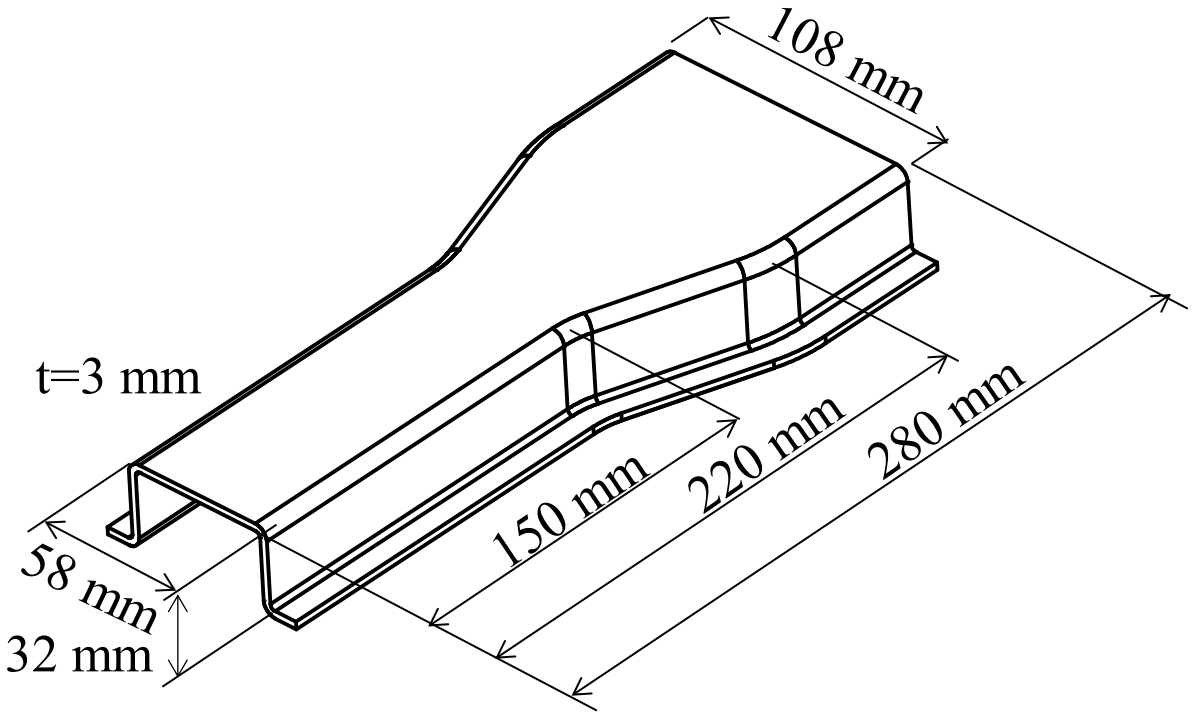

Figure 5. Geometry of the variant-cross-sectional-beam

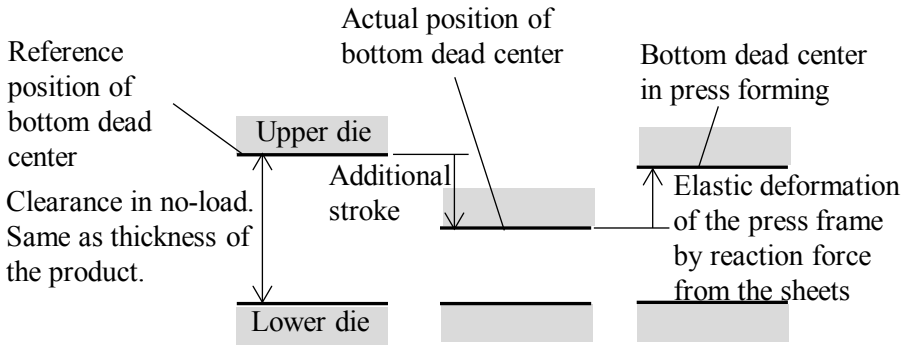

Figure 6. Assignment of additional strokes and the actual bottom dead center

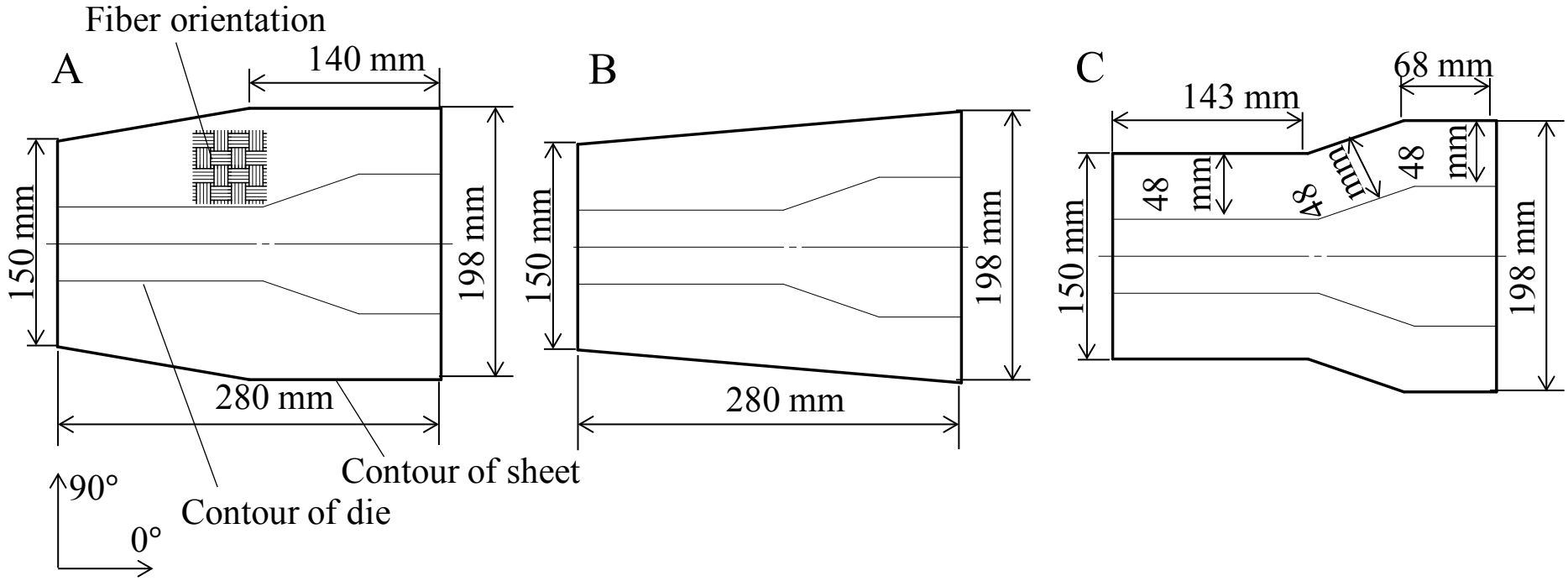

Figure 7. Sheet geometry

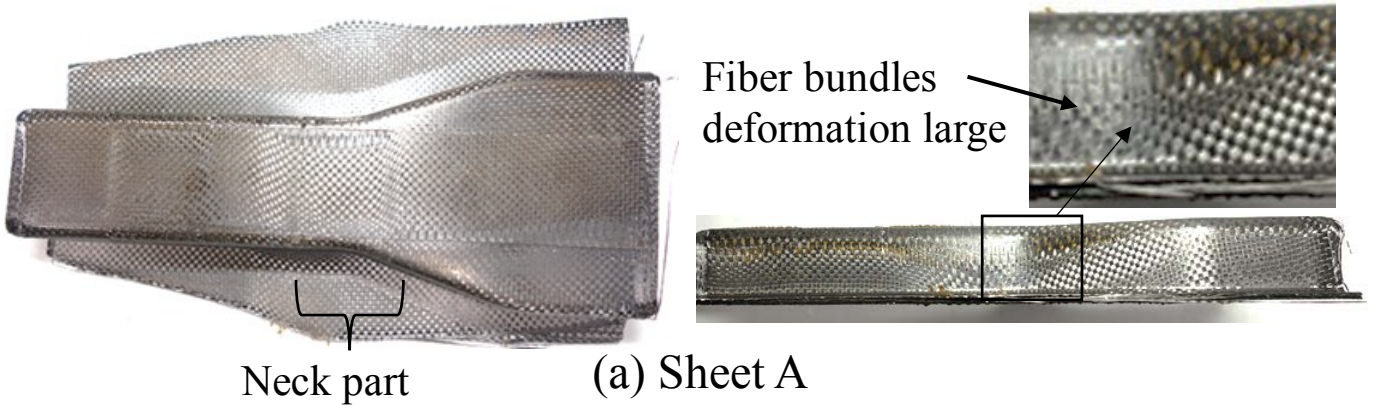

(a) Sheet A

(b) Sheet B

(c) Sheet C

Figure 8. Difference of fiber deformation owing to sheet geometry

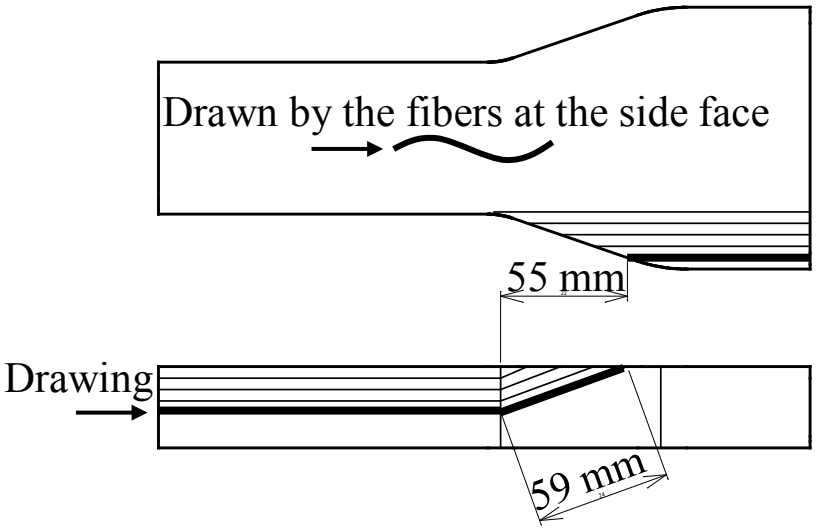

(a) Schema of fiber deformation

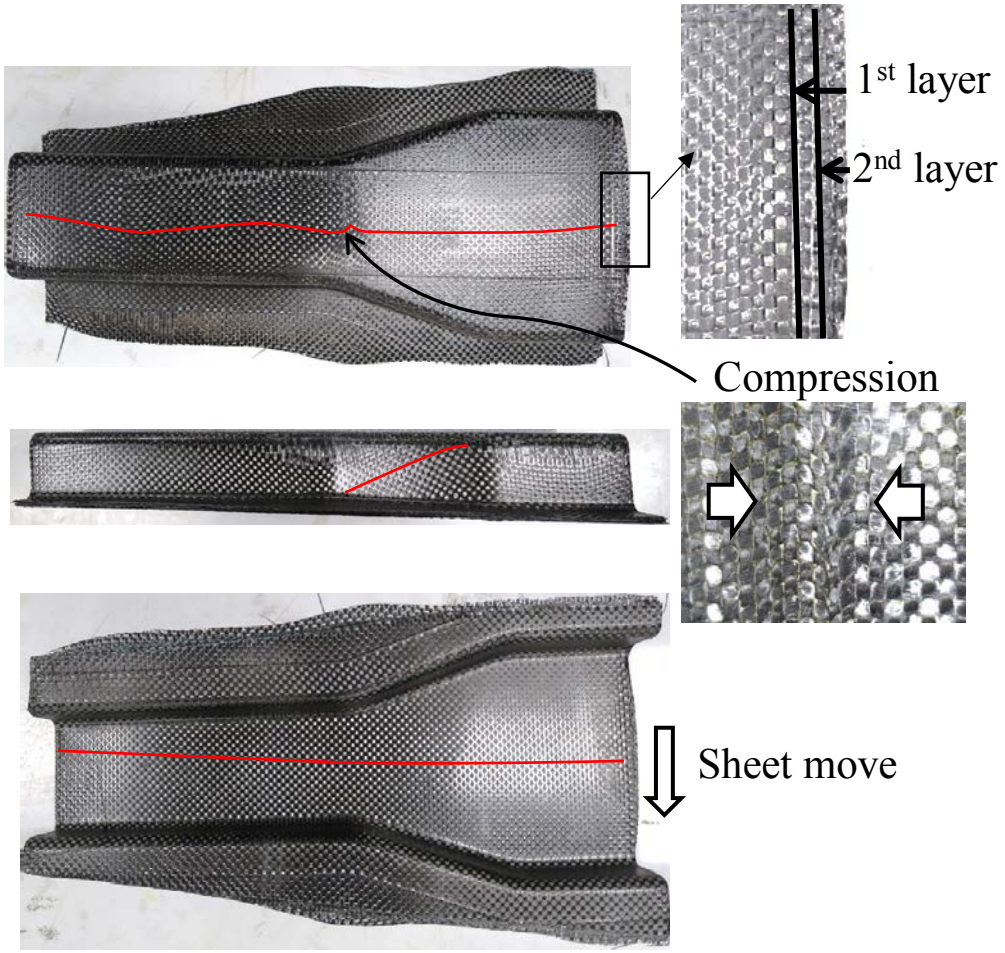

(b) Actual fiber deformation

Figure 9. Fiber deformation after press forming

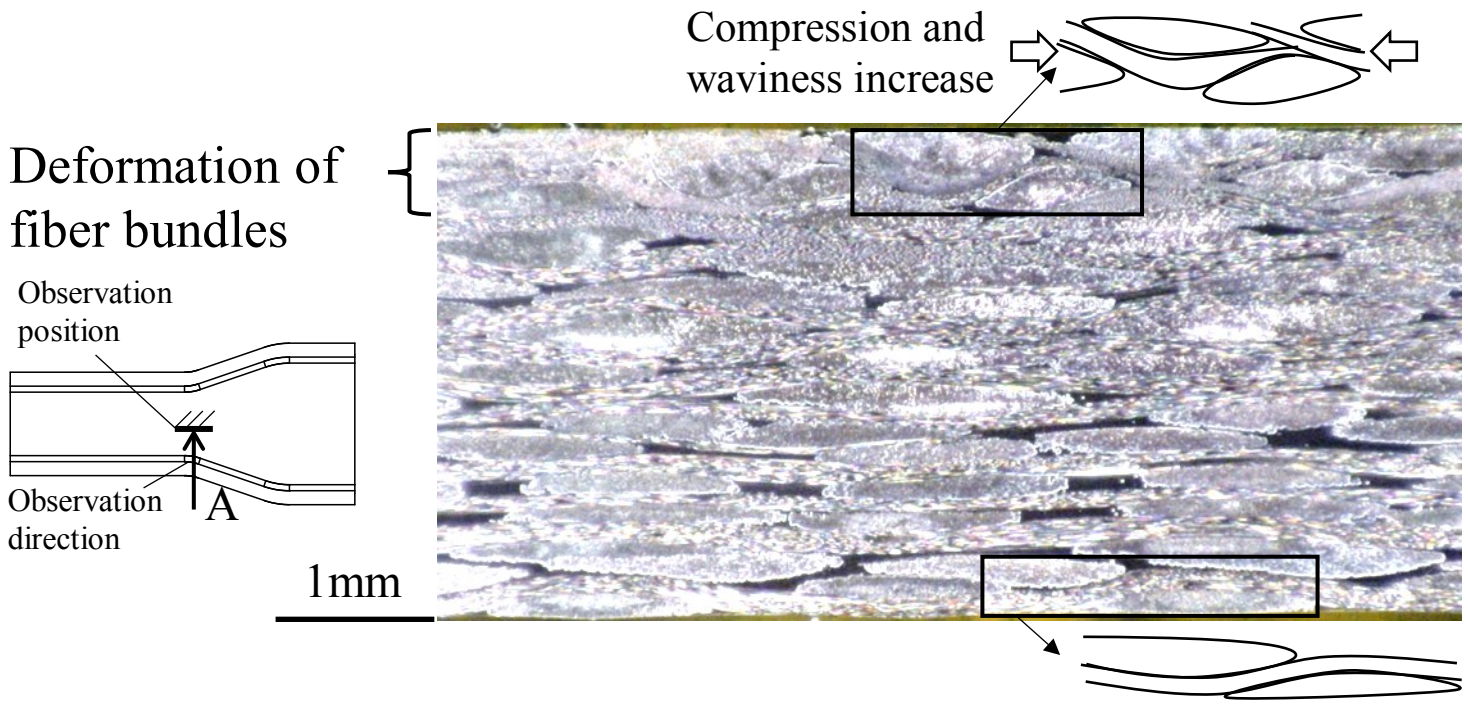

Figure 10. Inner structure (view A). Taken in high resolution using optical microscope

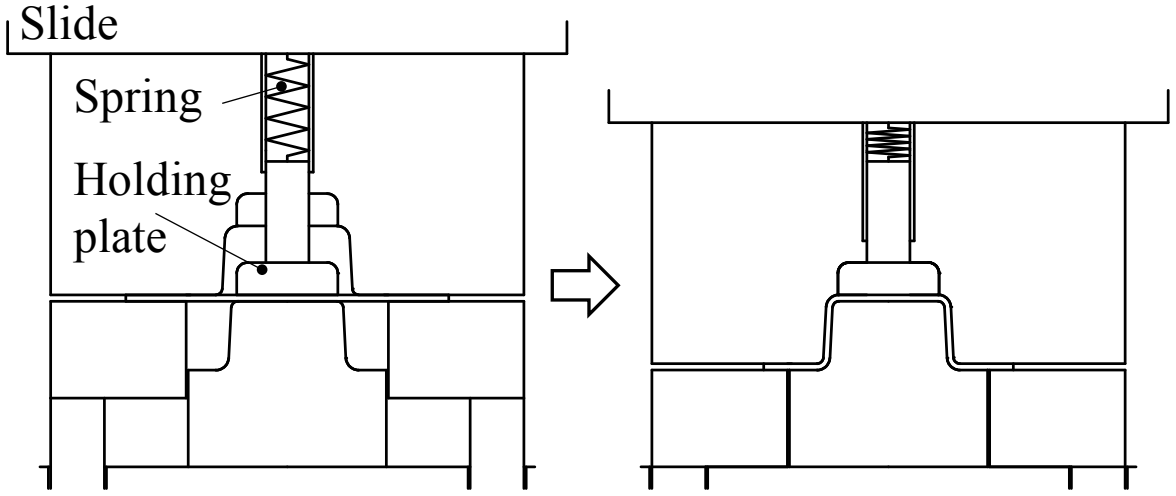

(a) Schematic of die structure

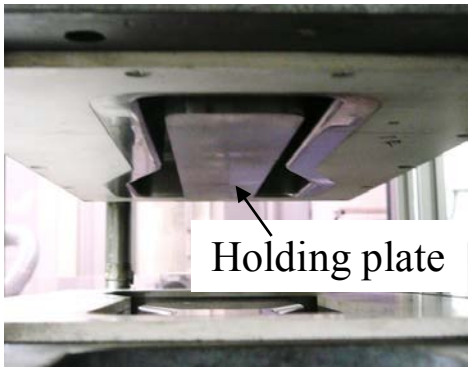

(b) Appearance of die

Figure 11. Mechanism of holding the sheet during press forming

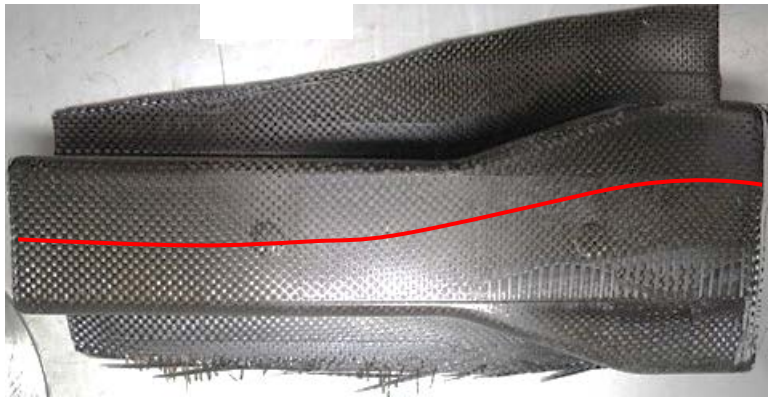

(a) Fiber deformation at the top

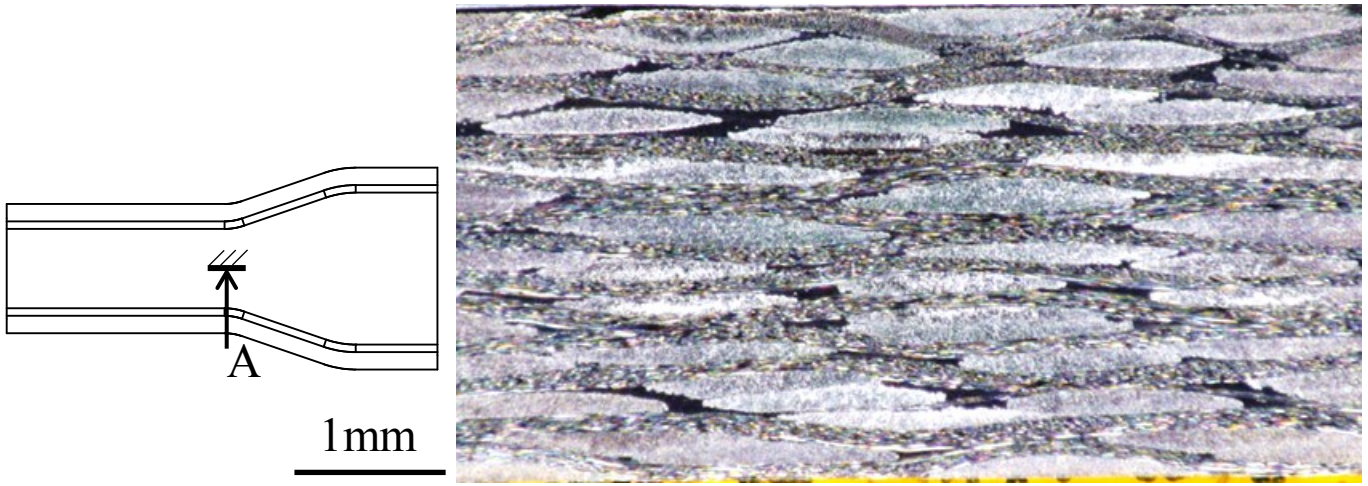

(b) Inner structure (view A), taken in high resolution using optical microscope

Figure 12. Result of press forming using the die with holding plate

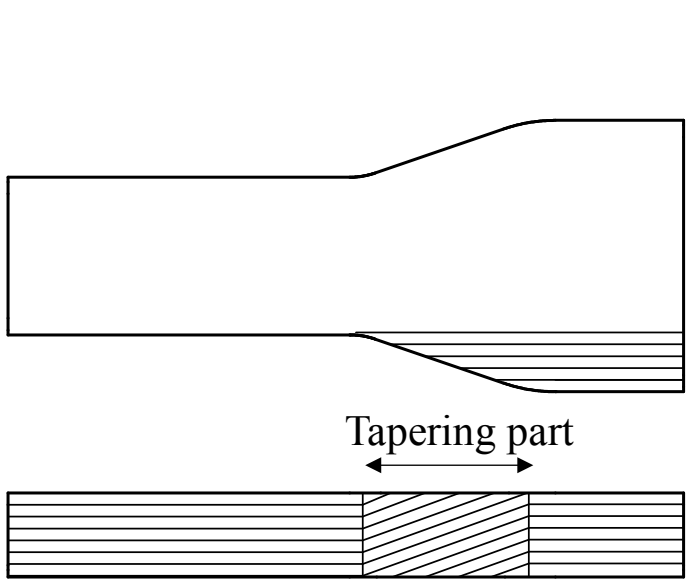

(a) Fiber direction at the tapering part using sheet with fibers are parallel to longitudinal direction of beam

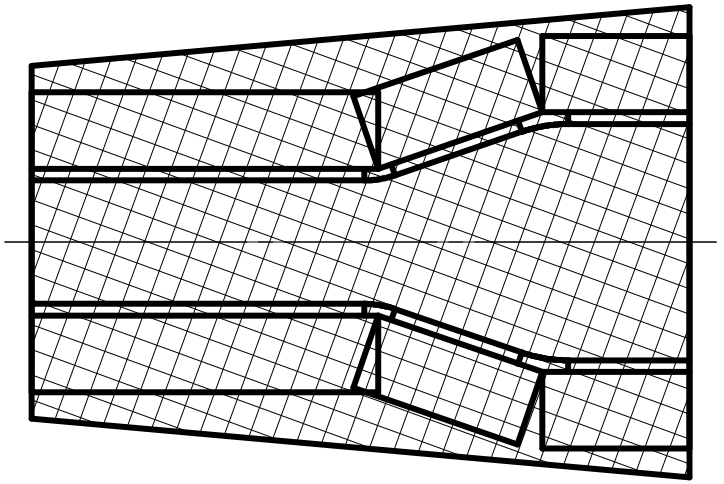

(b) Sheet with fibers are oriented to be parallel to the tapering part after being formed. Referred to as (-20/70) sheet

Figure 13. Fiber direction of the sheet considering the deformation caused by press forming

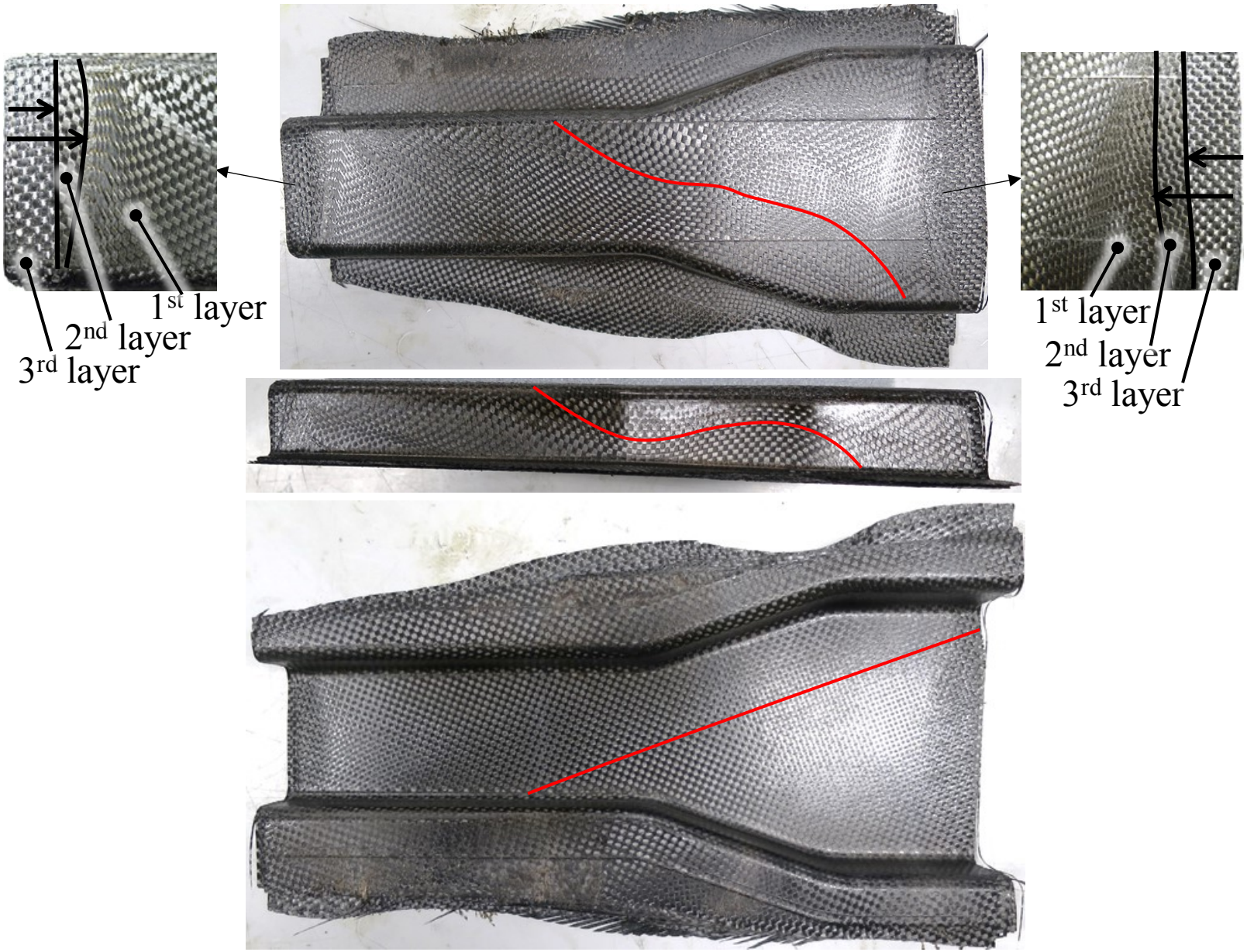

Figure 14. Forming result using (-20/70) sheets

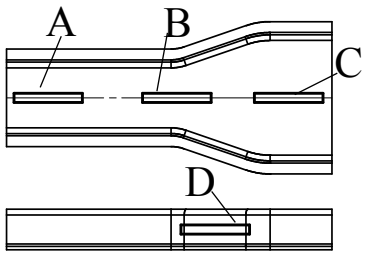

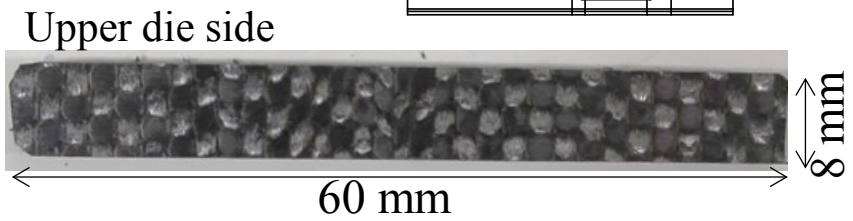

(a) (0/90) sheets only, specimen B

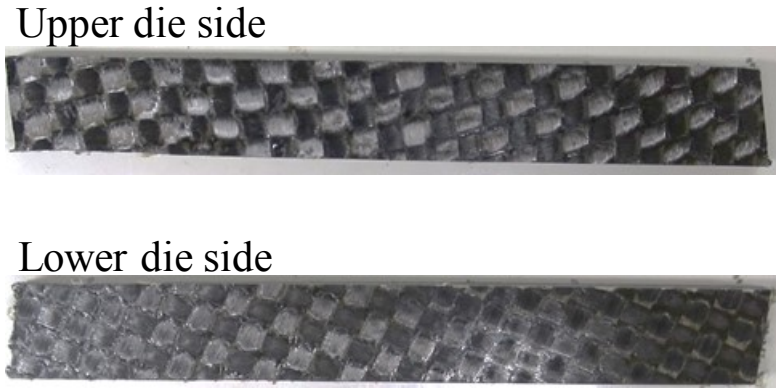

(b) (-20/70) sheets include, specimen B

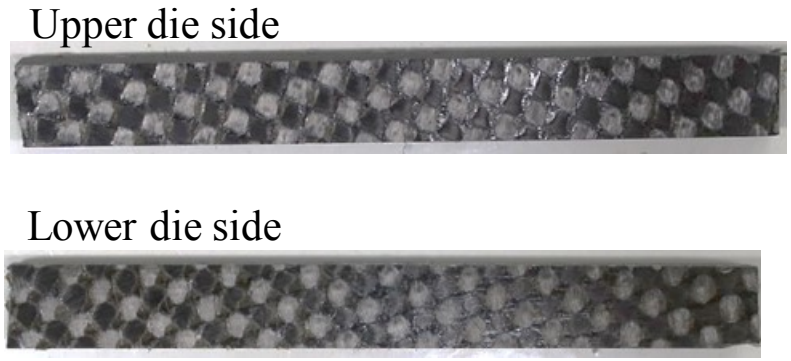

(c) (0/90) sheets only, specimen D

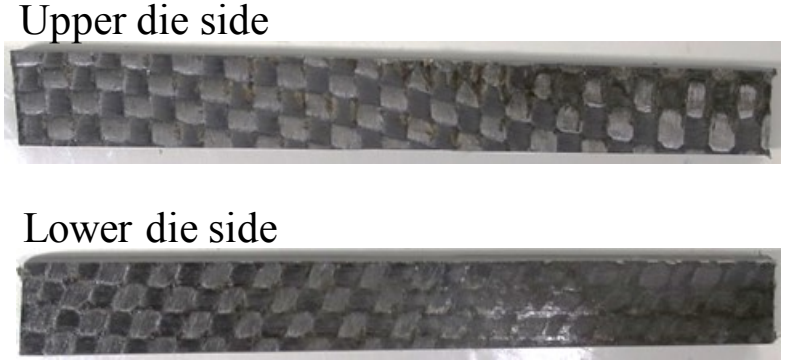

(d) (-20/70) sheets include, specimen D

Figure 15. Fiber orientation in the specimens in different fiber direction

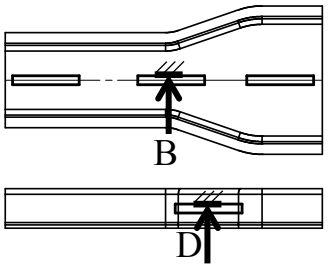

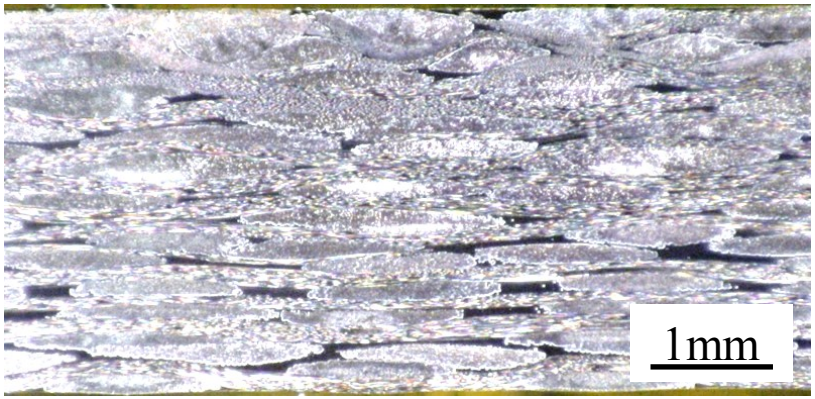

(a) (0/90) sheets only, section B

Fibers do not cross along the specimen

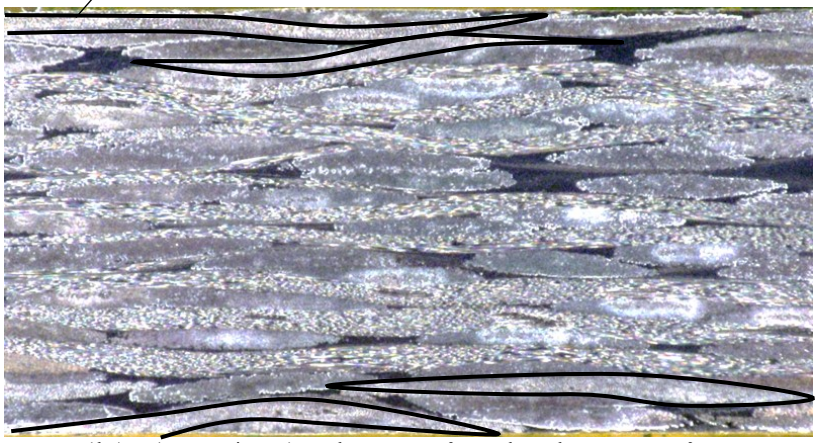

(b) (-20/70) sheets include, section B

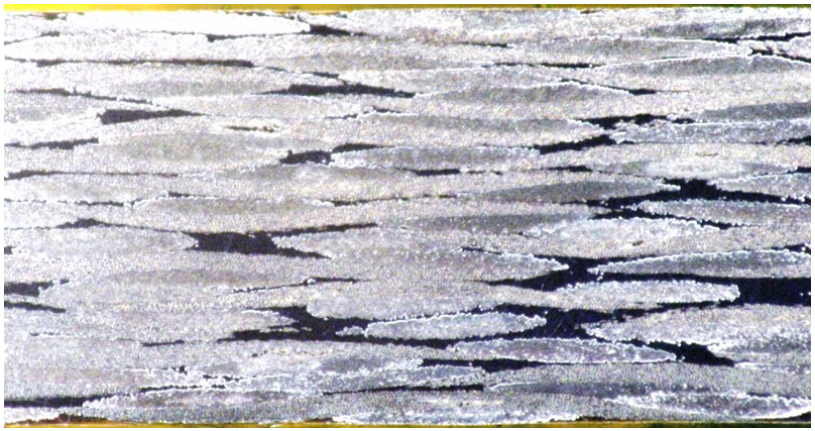

(c) (0/90) sheets only, section D

Fiber crossing along the specimen

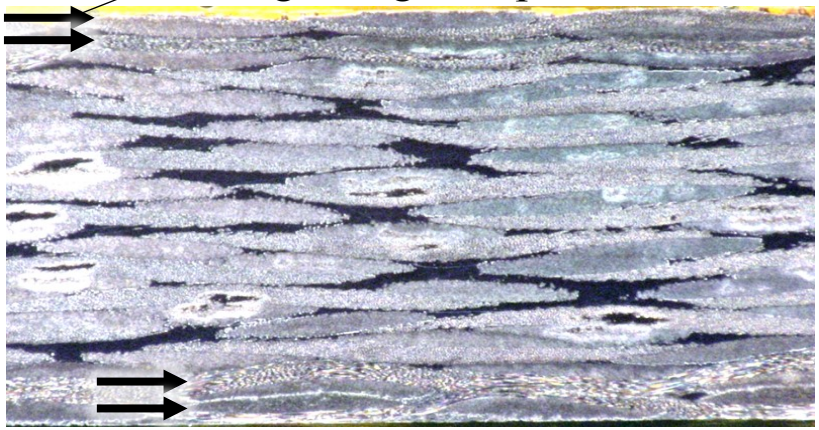

(d) (-20/70) include, section D

Figure 16. Difference in the inner structure due to the fiber direction. Taken in high resolution using optical microscope

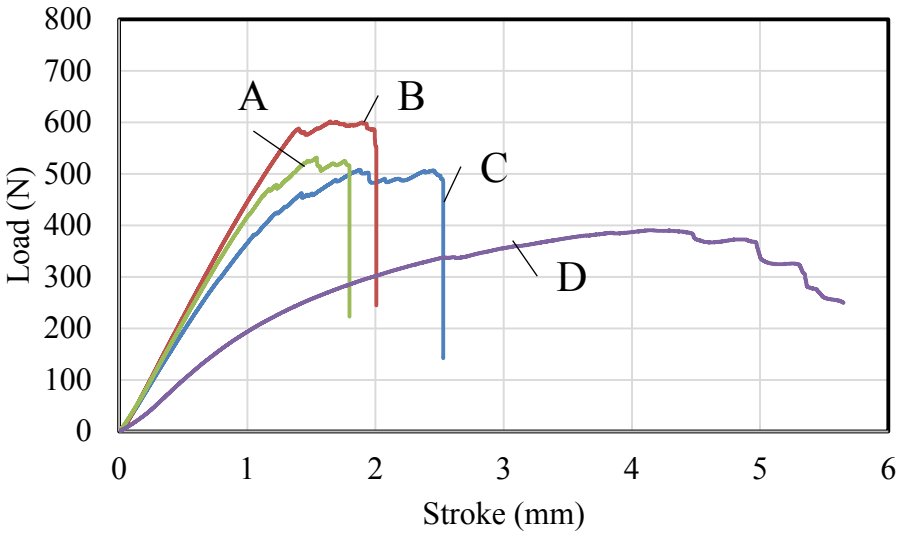

(a) Testing load curve of (0/90) sheets only

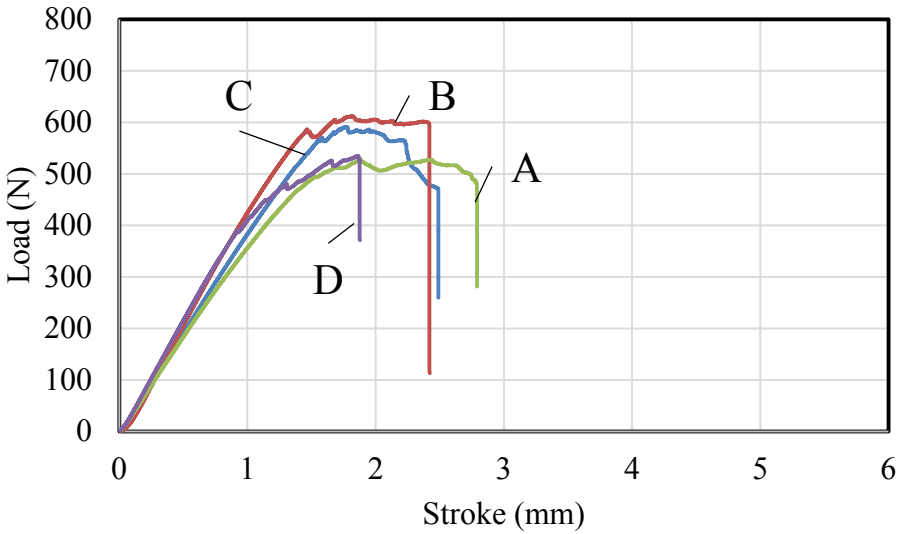

(b) Testing load curve of (-20/70) sheets include

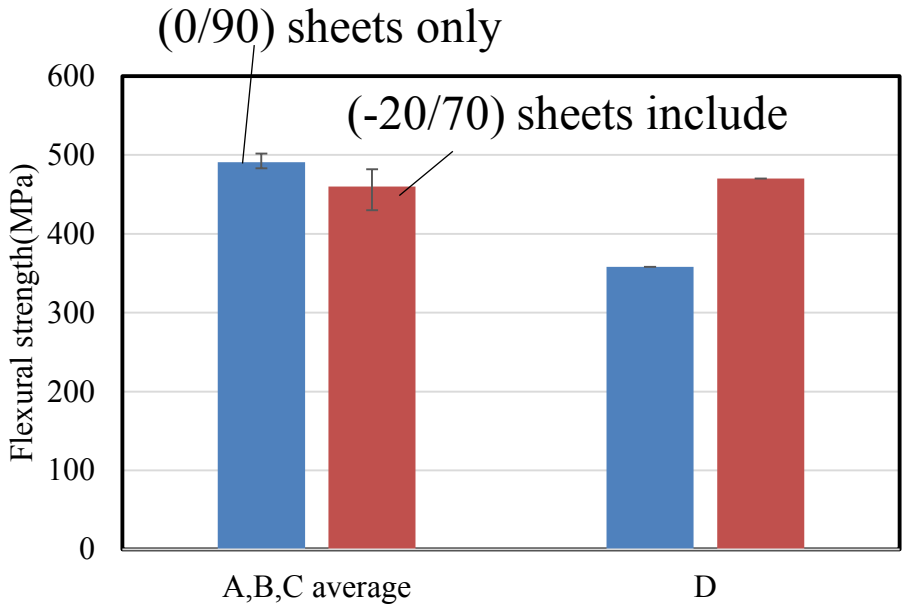

(c) Flexural strength

Figure 17. Result of flexural test in different fiber direction

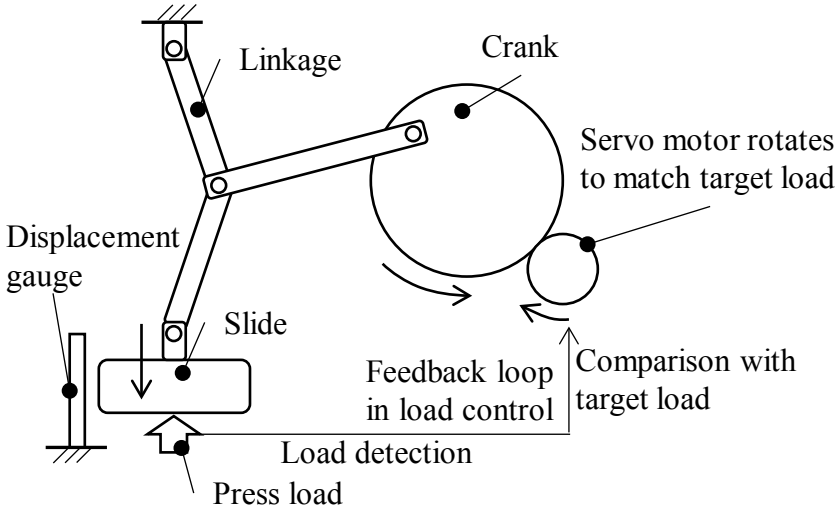

(a) Mechanism of servo press

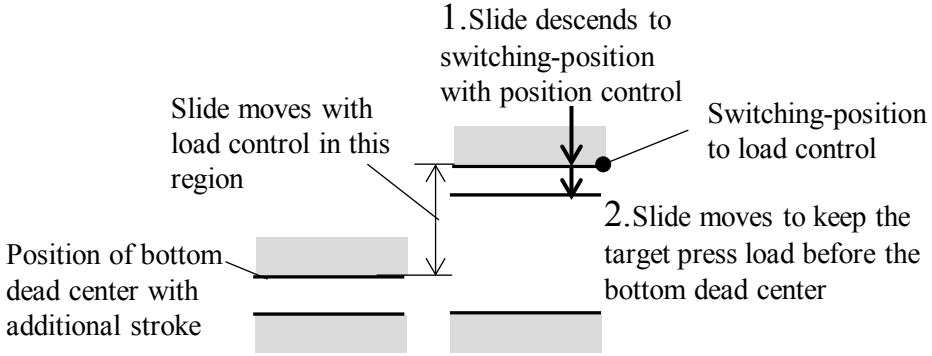

(b) Slide motion in load control

Figure 18. Slide motion in the load control operation

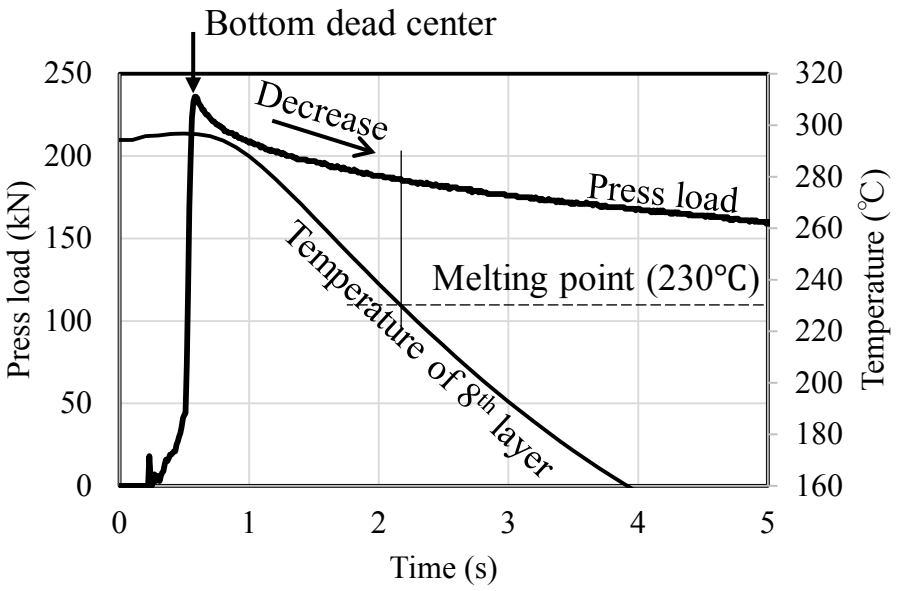

(a) Position control

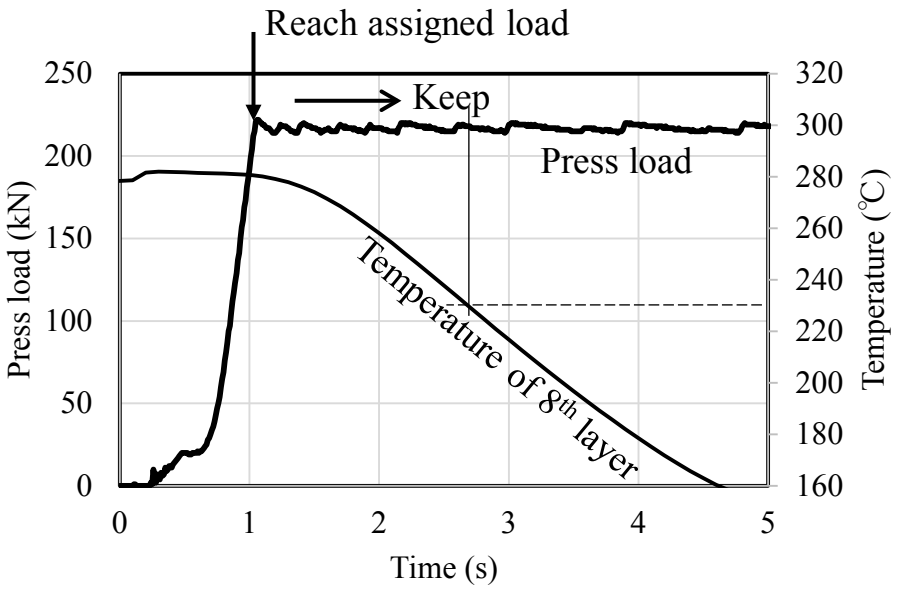

(b) Load control

Figure 19. Difference between press-load and temperature curves due to slide motion

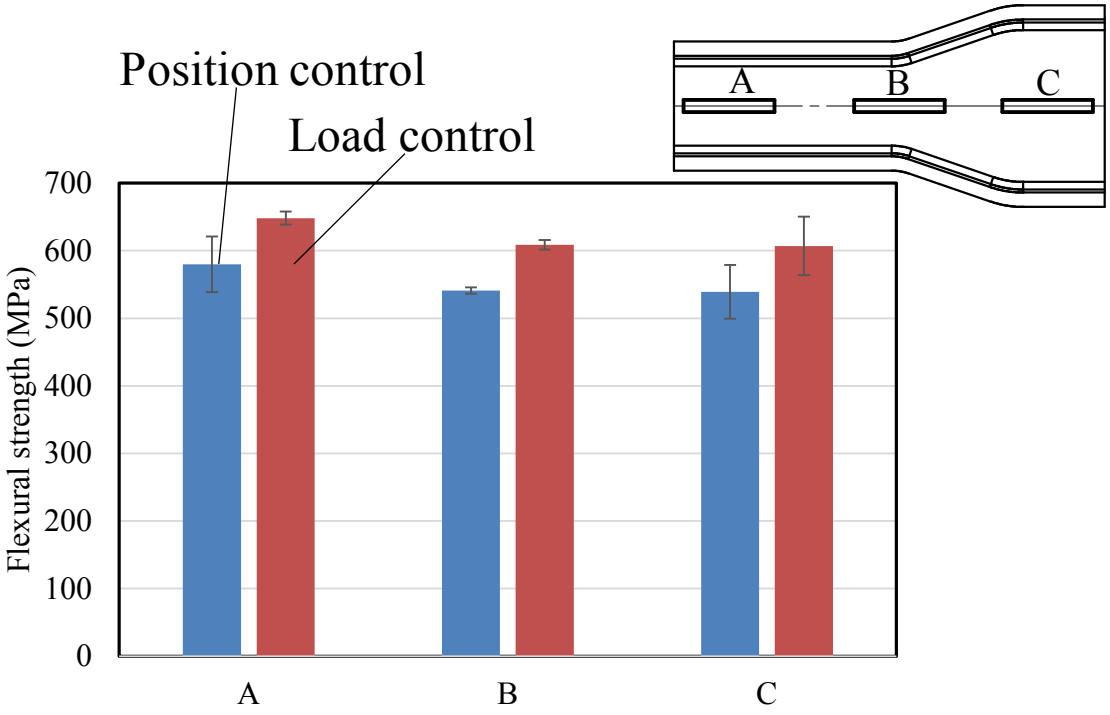

Figure 20. Difference between flexural strength due to slide motion

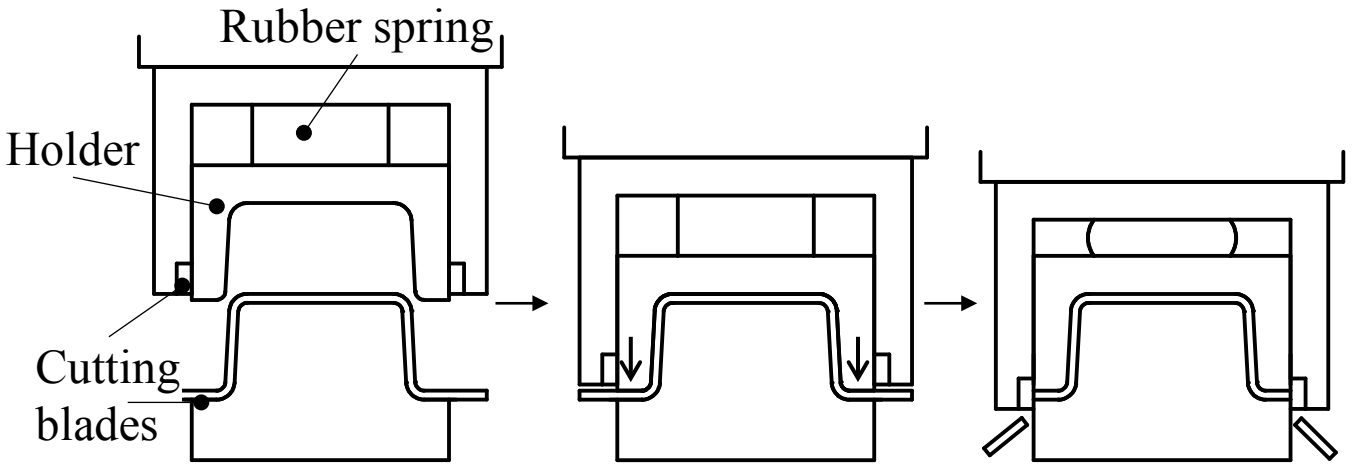

(a) Schematic of die structure

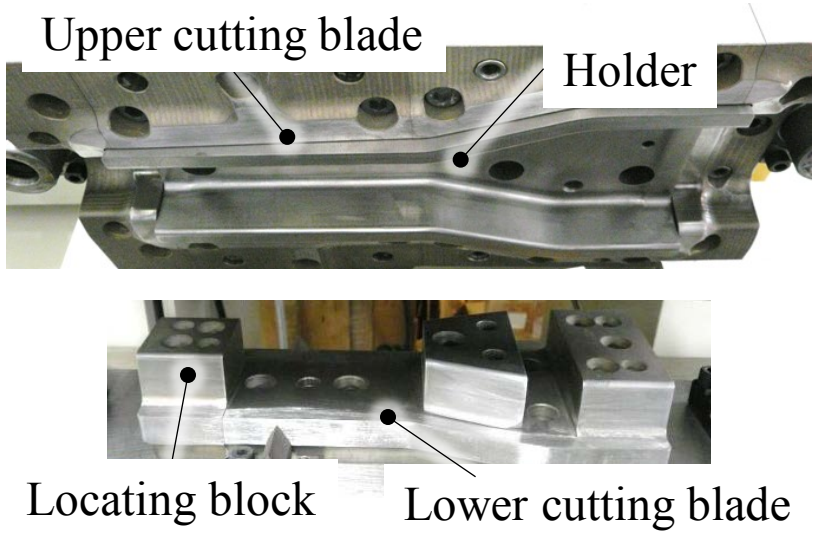

(b) Appearance

Figure 21. Shear-cutting die

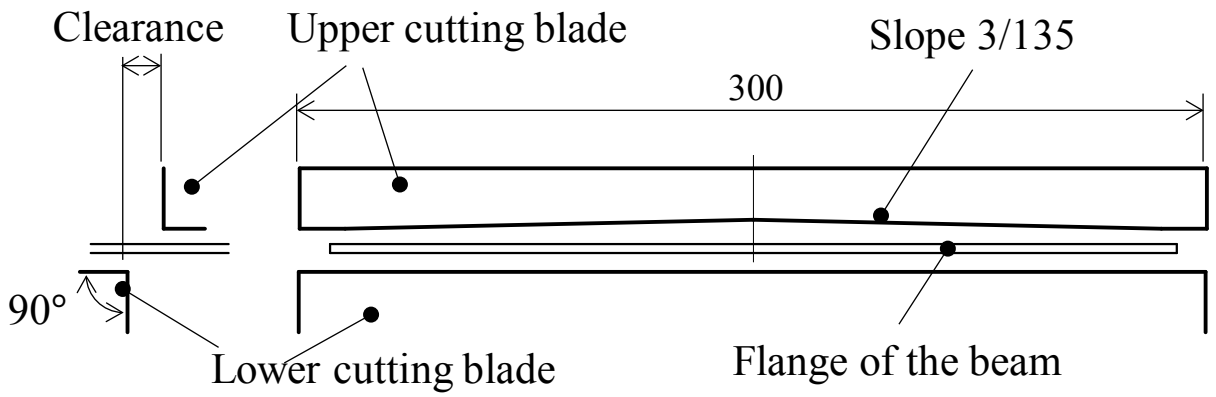

(a) Cutting blade view from the side

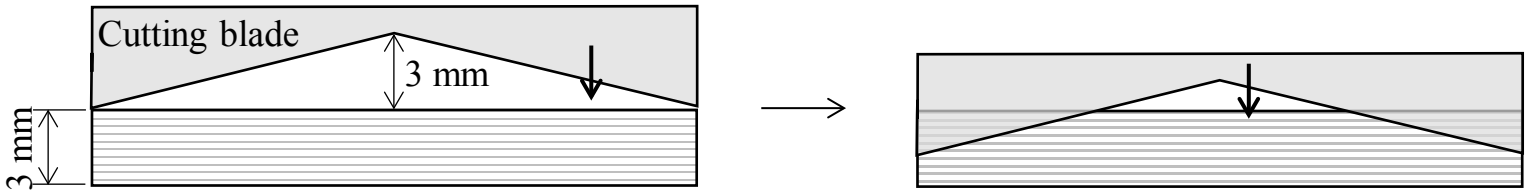

(b) Cutting process

Figure 22. Shape of cutting blades

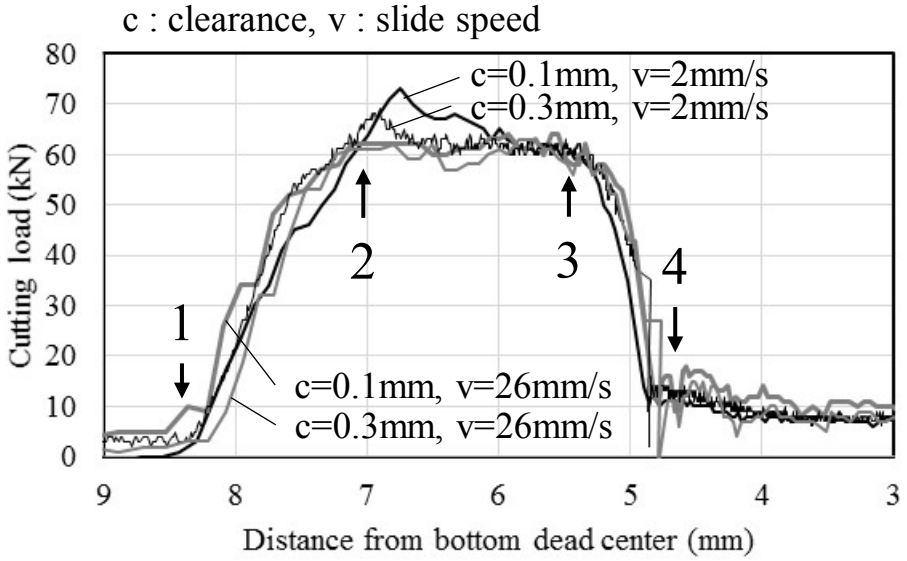

(a) Cutting load curve

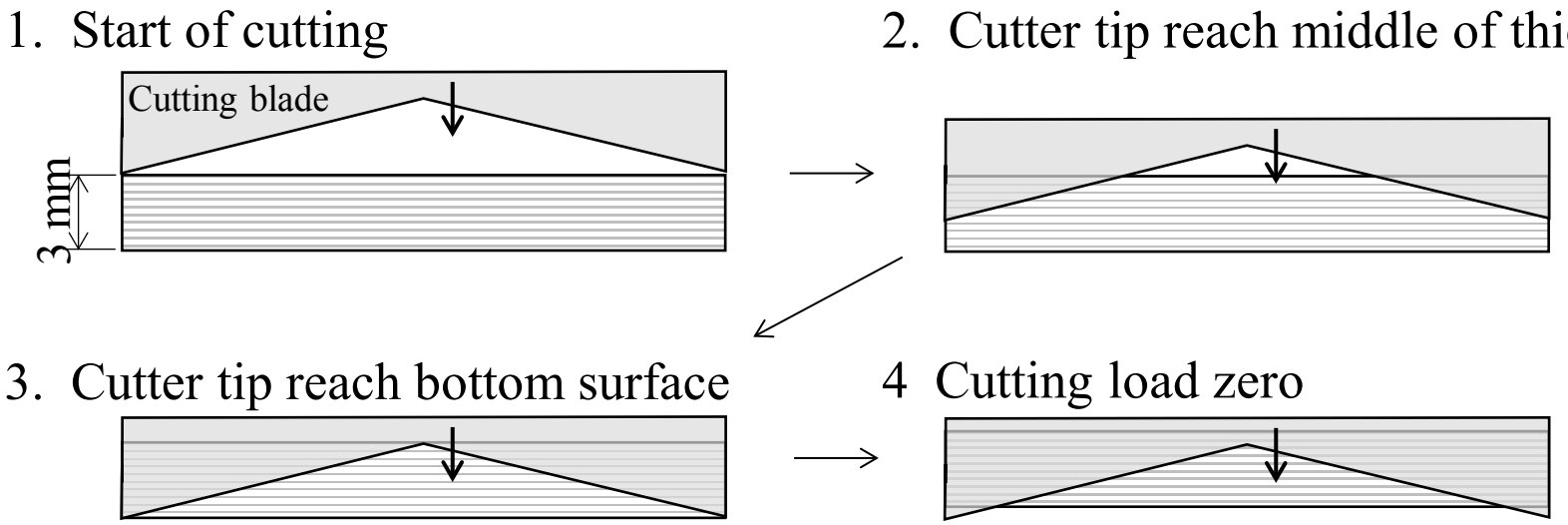

(b) Position of the cutting blade during shear-cutting

Figure 23. Relationship between cutting load and position of the cutting blade during shear cutting

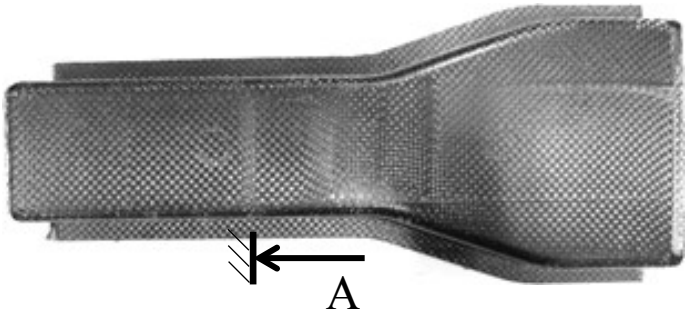

(a) Appearance after shear cutting

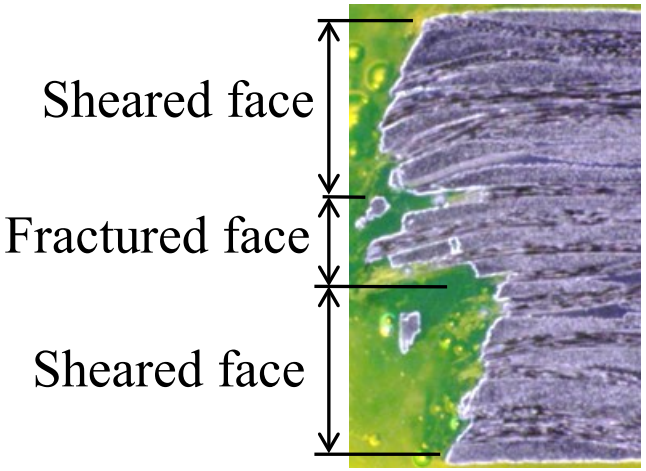

c=0.1 mm, v=2 mm/s

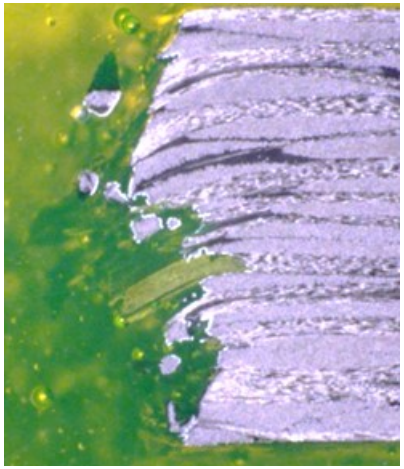

c=0.1 mm, v=26 mm/s

c=0.3 mm, v=2 mm/s

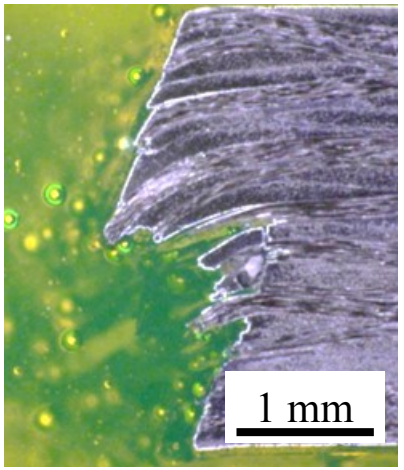

c=0.3 mm, v=26 mm/s

(b) Shape of the cut edge in different cutting conditions, view A

Figure 24. Result of shear cutting

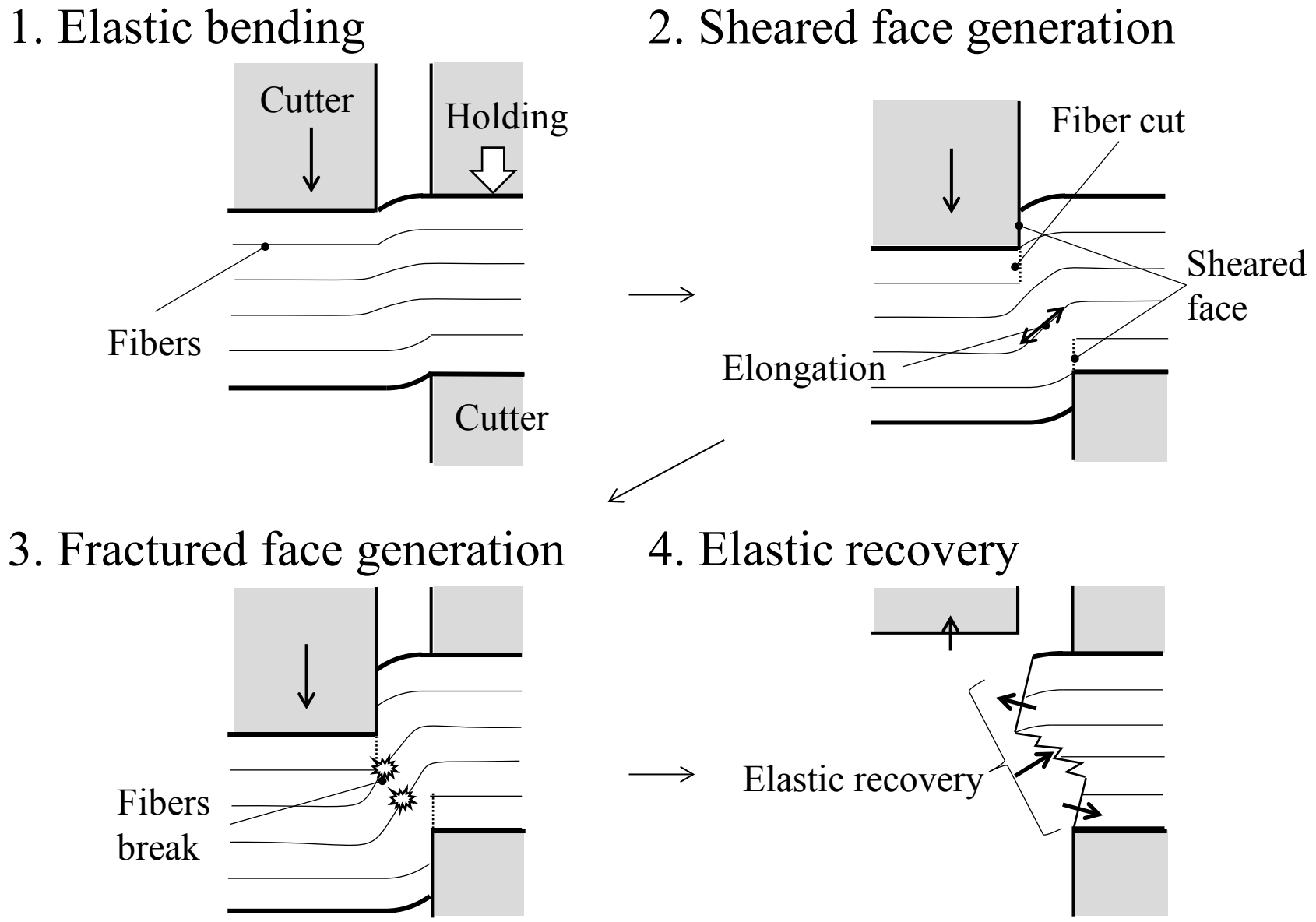

Figure 25. Estimation of shear cutting mechanism

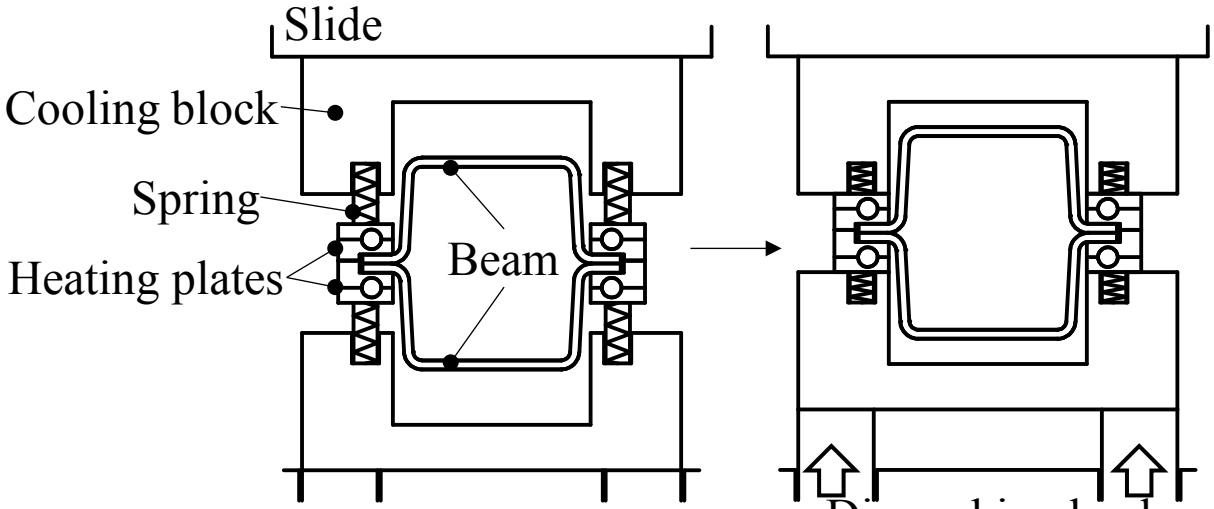

(a) Process of joining

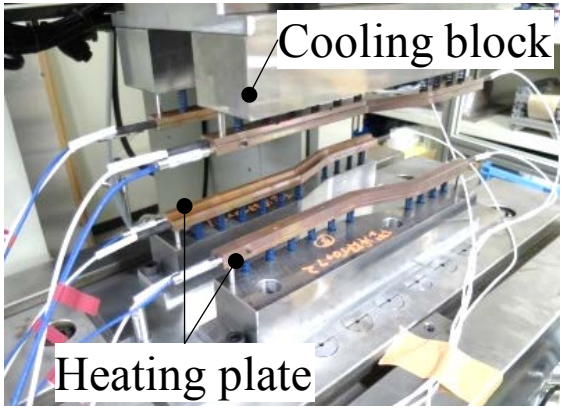

(b) Appearance of the die

Figure 26. Joining die

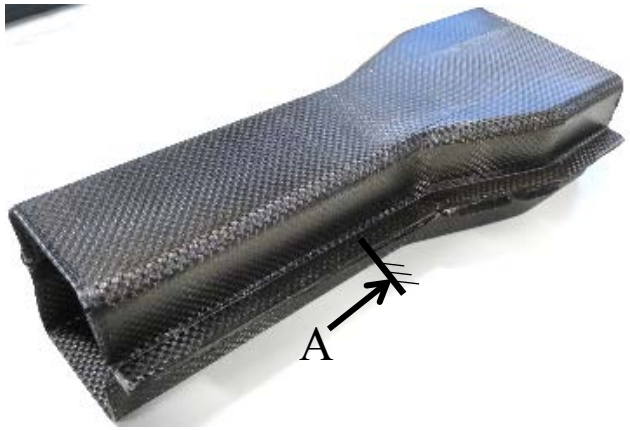

Front view Bird's eye view

(a) Appearance of joined closed-sectional-beam

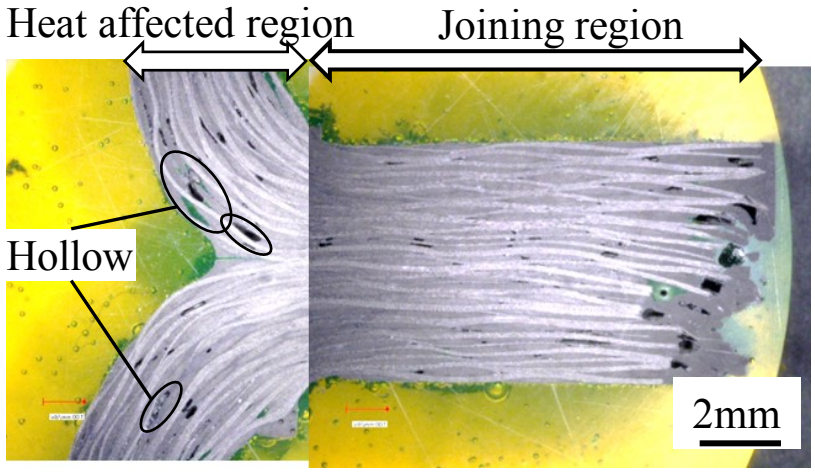

(b) Inner structure, view A

Figure 27. Result of joining